Arabian Journal of Chemistry (2020) 13, 632–648

King Saud University

Arabian Journal of Chemistry

www.ksu.edu.sa
www.sciencedirect.com

ORIGINAL ARTICLE

Quinoline derivatives as possible lead compounds for anti-malarial drugs: Spectroscopic, DFT and MD study

Bhaskaran Sureshkumar [a], Yohannan Sheena Mary [b], Chacko Yohannan Panicker [b], Somasekharan Suma [a], Stevan Armaković [c,*], Sanja J. Armaković [d], Christian Van Alsenoy [e], Badiadka Narayana [f]

[a] *Department of Chemistry, SN College, Kollam, Kerala, India*
[b] *Department of Physics, Fatima Mata National College, Kollam, Kerala, India*
[c] *University of Novi Sad, Faculty of Sciences, Department of Physics, Trg D. Obradovića 4, 21000 Novi Sad, Serbia*
[d] *University of Novi Sad, Faculty of Sciences, Department of Chemistry, Biochemistry and Environmental Protection, Trg D. Obradovića 3, 21000 Novi Sad, Serbia*
[e] *Department of Chemistry, University of Antwerp, Groenenborgerlaan 171, B-2020 Antwerp, Belgium*
[f] *Department of Chemistry, Mangalore University, Mangalagangothri, Mangaluru, Karnataka, India*

Received 25 April 2017; accepted 10 July 2017
Available online 18 July 2017

KEYWORDS

Quinoline;
DFT;
ALIE;
BDE;
RDF;
Molecular docking

Abstract In this work we report spectroscopic characterization and reactivity study by density functional theory (DFT) and molecular dynamics (MD) simulations of two quinoline derivatives. Collected computational results for the two new derivatives have been compared with the pristine quinoline in order to investigate the consequences of modifications by introduction of chlorine atoms and methyl and OH groups. Potential energy distribution (PED) analysis has been performed in order to assign principal vibrational numbers. DFT calculations have been used to obtain global and local quantum-molecular descriptors including frontier molecular orbitals, charge distribution by molecular electrostatic potential (MEP) surface, average local ionization energy (ALIE) surface, and Fukui functions. Natural bond order (NBO) analysis has been performed in order to investigate hyper-conjugative properties. To investigate sensitivity towards autoxidation and hydrolysis we have calculated bond dissociation energies (BDE) and radial distribution functions (RDF). Molecular docking study has also been performed in order to initially assess the potential of target

* Corresponding author.
E-mail addresses: bskumar2943@gmail.com (B. Sureshkumar), sypanicker@rediffmail.com (Y.S. Mary), cyphyp@rediffmail.com (C.Y. Panicker), suma_jaykay@yahoo.co.in (S. Suma), stevan.armakovic@df.uns.ac.rs (S. Armaković), sanja.armakovic@dh.uns.ac.rs (S.J. Armaković), kris.vanalsenoy@uantwerpen.be (C. Van Alsenoy), nbadiaka@yahoo.co.uk (B. Narayana).
Peer review under responsibility of King Saud University.

Production and hosting by Elsevier

http://dx.doi.org/10.1016/j.arabjc.2017.07.006

molecules to bind with dehydrogenase inhibitor and these quinoline derivatives can be a lead compounds for developing new anti-malarial drug.

1. Introduction

Quinoline derivatives are probably best known for their diverse pharmacological properties (Marella et al., 2013), however they have also been successfully applied as optical switches in nonlinear optics, sensors in electrochemistry and in the field of inorganic chemistry (Khan et al., 2014; Sangani et al., 2014). Among other reasons, quinoline derivatives owe their popularity due to the fact that quinoline ring is readily available through synthesis by series of methods (Kumar et al., 2009), while modern methods of its synthesis include application of metallic and organometallic reagents (Swenson et al., 2002; Cho et al., 1999; Makioka et al., 1995; Sangu et al., 2004; Crousse et al., 1998). Some of the most important biological activities of quinoline derivatives include anticancer (Afzal et al., 2015) and antimalarial (Kumar et al., 2009; Afzal et al., 2015; Wright et al., 2001) activities, while many different derivatives with anti(myco)bacterial Senthilkumar et al., 2009, anticonvulsant (Guo et al., 2009), antiinflammatory (Calhoun et al., 1995), cardiovascular (McCall et al., 1986; Sircar et al., 1992) activities(Kumar et al., 2009; Afzal et al., 2015; Wright et al., 2001) have been synthetized as well. Afzal et al. (2015) have mentioned eight anticancer drugs containing quinoline unit, while their efficiency in this context is owed to the fact that they can have different action mechanisms. Some chloroquinoline derivatives even exhibit anti-leishmanial (Hussain et al., 2002) properties. Taha et al. have synthesized two large groups of novel quinoline based derivatives and evaluated their potential as β-glucuronidase and α-glucosidase inhibitors (Taha et al., 2015, 2016).

In the area of materials science, quinoline derivatives are important due to the fact that some of them exhibit important properties optical and sensing properties. For example, hydroxyquinoline derivatives are commonly used for chelating metal cations and have fluorescent properties (Perez-Bolivar et al., 2006; Wang et al., 2001a, 2001b; Mulon et al., 2005), while some quinoline derivatives are used for quantification of metal ions (Mameli et al., 2010; Park et al., 2011). Photoluminescence from 8-hydroxy quinoline aluminum embedded in porous anodic alumina membrane has been reported by Huang et al. (2005). Mphahlele and Adeloye (2013) have synthetized and investigated photophysical properties, particularly solvent-dependent emission characteristics, of some 4,6,8-triarylquinoline-3-carbaldehyde derivatives and suggested the intramolecular charge transfer character of the emission state. Mi et al. (2014) have demonstrated highly selective Al^{3+} and F^{-} sensing properties of rhodamine-quinoline based molecular switch, while da Rocha et al. (2016) have investigated kinetic and thermodynamic parameters of some 2-amino-1,4-naphthoquinone derivatives demonstrating that naphthoquinone derivatives could be considered as promising fluorescent probes.

Computational molecular modeling approaches have been employed for the investigation of reactive properties of various organic molecules and nanostructures (Giacoppo et al., 2017; Menon et al., 2017; Ramalho et al., 2009, 2004; Khavani et al., 2017). Quantities calculated by DFT calculations and MD simulations help scientists to evaluate, for example, stability of molecules, which can be of particular importance for understanding of degradation properties of molecules. Elimination of organic molecules is of high importance through degradation as various conventional methods are not quite sufficient that leads us to perform the degradation study (Armaković et al., 2012, 2015; Blessy et al., 2014). For these purposes forced degradation procedures based on advanced oxidation processes are seen as adequate and efficient alternatives (Armaković et al., 2015, 2016, 2019; Abramović et al., 2011; Molnar et al., 2011; Molnar et al., 2012; Četojević-Simin et al., 2013). DFT calculations and MD simulations are frequently used, which provides sufficient knowledge about the confined reactivity properties that play vital role in improvements of these procedures (Lienard et al., 2015; de Souza et al., 2016; Sroka et al., 2015; Djeradi et al., 2014).

In the present study we have compared various quantum-molecular descriptors of 8-hydroy-2-methyl quinoline (**2**) and 5,7-dichloro-8-hydroy-2-methyl quinoline (**3**) with pristine quinoline (**1**), in order to locate possibly important reactive molecule sites. Among quantities reflecting global and local reactivity properties such as HOMO-LUMO gap, MEP and ALIE surfaces, Fukui functions, we have also calculated and analyzed bond dissociation energies (BDE) and radial distribution functions (RDF) in order to understand sensitivity towards autoxidation and hydrolysis mechanisms, which are important for the degradation properties. Charge transfer as a consequence of the lowest energy excitation has been also addressed.

2. Experimental and computational details

Fine samples of the title compounds were obtained from Sigma Aldrich®, USA and used without any further purification for spectral measurements. The FT-IR spectra (Fig. S1) of the title compounds were recorded in the region 4000–400 cm^{-1} using Perkin Elmer RX1 spectrometer equipped with Helium-Neon laser source, potassium bromide beam splitter and $LiTaO_3$ detector. The FT-Raman spectra (Fig. S2) of the title compounds were recorded in 4000–0 cm^{-1} with a Nicolet model 950 FT-Raman spectrometer at 4 cm^{-1} spectral resolution using the 1064 nm line of a Nd:YAG laser for excitation at a 200 mW output power.

Calculations of the wavenumbers, molecular geometry, polarizability values, frontier molecular orbital analysis were carried out with Gaussian 09 program (Frisch et al., 2010) using the B3LYP/6-311++G(d) (5D, 7F) quantum chemical calculation method. A scaling factor of 0.9613 is used to scale the theoretically obtained wavenumbers (Foresman, 1996) and the assignments of the vibrational wavenumbers are done by using GaussView (Dennington et al., 2009) and GAR2PED software (Martin and Van Alsenoy, 2007). Good agreement between experiment and theory served us to validate the used level of theory.

DFT calculations have been also performed with Jaguar 9.4 (Bochevarov et al., 2013) program, while MD simulations have been performed with Desmond (Shivakumar et al., 2010; Guo et al., 2010; Bowers et al., 2006; Bregović et al., 2015) program. Both Jaguar and Desmond programs were used as implemented in Schrödinger Materials Science Suite 2016-4 (SMSS). B3LYP exchange-correlation functional (Becke, 1993) has been employed also for DFT calculations with Jaguar, with the following choices on basis sets: 6-311++G(d,p), 6-31+G(d,p) and 6-311G(d,p) for the calculations of ALIE, Fukui functions and BDEs, respectively. For MD simulations the latest variant of OPLS force field, namely the OPLS 3, was used (Shivakumar et al., 2010; Harder et al., 2015; Jorgensen et al., 1996; Jorgensen and Tirado-Rives, 1988). Simulation time was set to 10 ns, while temperature was set to 300 K. Pressure was

1.0325 bar, while cut off radius was 10 Å. System was of isothermal–isobaric (NPT) ensemble class. For the solvent a simple point charge (SPC) model Berendsen et al., 1981 was used. MD simulation was done by placing of one target molecule into the cubic box with ~2000 water molecules. Electron density analysis for the purpose of determination of intramolecular noncovalent interactions has been done employing methods by Otero-de-la-Roza et al. (2012), Johnson et al. (2010). Maestro GUI (Schrödinger Release 2016-4, 2016) was used for the preparation of input files and analysis of results when Schrödinger Materials Science Suite 2016-4 was employed. High resolution crystal structure of dehydrogenase inhibitor was downloaded from the RSCB protein data bank website with PDB ID: 5TBO (Phillips et al., 2016; Berman et al., 2000, 2003; Bernstein et al., 1977, 1978; Bank, 1971).

3. Results and discussion

In the following discussion, the rings, C1—C2—C3—C4—C5—C6 and N7—C8—C9—C10—C5—C4 (Fig. 1) of quinoline (**1**), 8-hydroy-2-methyl quinoline (**2**) and 5,7-dichloro-8-hydroy-2-methyl quinoline (**3**) are designated as PhI and PhII, respectively. A very important step in computational studies of molecules should be a proper choice of conformations for geometrical optimizations. In order to obtain possible conformations MD simulations can be performed, however this process, although very efficient, sometimes produces great number of conformations, which prolongs the identification of the most relevant structures. In order to treat the problem of large number of conformations obtained by MD simulations, many theoretical methods have been developed (van der Wijst et al., 2009; Coutinho et al., 2000), while the most common methods are based on the random selection (Mancini et al., 2014; Tachikawa et al., 2002). Very recently, a new method based on the wavelet analysis, called optimal wavelet signal compression algorithm (OWSCA) has been developed by Gonçalves et al. (2017).

However, taking into account the size and structures of molecules investigated in this work, significant number of conformations was not expected. Concretely, molecule **1** has flexible bonds, while **2** and **3** have two relatively flexible bonds. Using the MacroModel program (Schrödinger Release 2017-2), as implemented in SMSS, and OPLS3 force field we have performed conformational search in order to assure that there are no significant amount conformations, including the solvent effects. With and without solvent effects, conformational search yielded only one conformation of **1** and **3**, and two conformations of **2**. In case of the **2**, the more stable one was taken into account for further investigation. Taking into account the conformational search with and without the influence of water, it can be concluded that the conformational space of structures investigated in this work is very poor and that water as solvent has no significant influence to structural properties of **1**, **2** and **3**. After geometrical optimization the following structures of **1**, **2** and **3** have been obtained, Fig. 1.

4. Geometrical parameters

The C2—C3 bond lengths of the title compounds are 1.3781 and 1.3798 Å, which are less than that of C4—C3 (1.4269 and 1.4276 Å) because of the delocalization of electrons due to the presence of C—OH group. Also the bond length of C1—C6 (1.3777 and 1.3730 Å) is less than that of C5—C6 (1.4168 and 1.4183 Å) owing to the delocalization of electrons. The large value of the bond length of C_4—C5 (1.4211 and 1.4222 Å) is due to the delocalization of electron density due to the adjacent quinoline ring. The C4-N7 and C8-C7 bond lengths of compounds were 1.3608, 1.3594 and 1.3190, 1.3191 Å respectively while reported value of similar deriva-

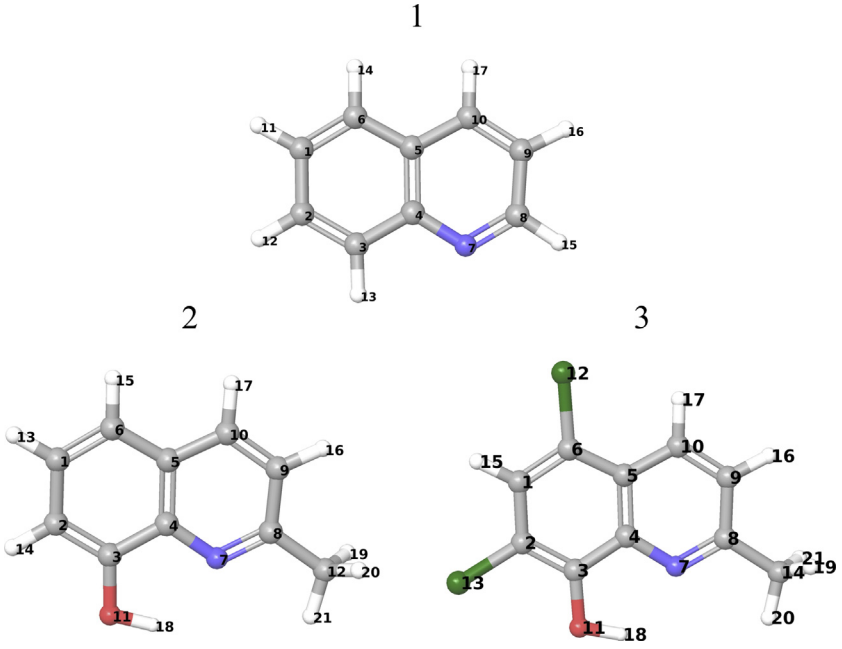

Fig. 1 Optimized geometries of pristine quinoline (**1**), its derivative with methyl and OH groups (**2**) and its derivative with methyl and OH groups, and chlorine atoms (**3**).

tives were 1.3874, 1.3345 (Merritt and Duffin, 1970), 1.3662, 1.3202 (Muthiah and Murugesan, 2006) and 1.3626, 1.3187 Å (Smith et al., 2007).

4.1. IR and Raman spectra

In order to validate the used level of theory we have compared experimentally and computationally obtained IR and Raman spectra. The observed experimental wavenumbers and vibrational assignments of compounds **2** and **3** are presented in Table S1 of the supplementary materials.

For the hydroxyl group, the OH group provided three normal vibrations; the stretching vibration OH, in-plane and out-of-plane deformations of OH. The in-plane OH deformation (Roeges, 1994) is expected in the region 1440 ± 40 cm^{-1} and the bands at 1410 cm^{-1} in the Raman spectrum, 1413 cm^{-1} (DFT) and 1410 cm^{-1} in the Raman spectrum, 1412 cm^{-1} (DFT) are assigned as the in-plane OH deformation modes for **3** and **2**, respectively. The stretching of hydroxyl group C—O appears at 1232 cm^{-1} (IR), 1228 cm^{-1} (DFT) for **3** and 1240 cm^{-1} (experimental), 1237 cm^{-1} (DFT) for **2** and this bands are not pure, but contains significant contributions from other modes also. This band is expected in the region 1220 ± 40cm^{-1} (Colthup et al., 1990; Silverstein et al., 1991). The out-of-plane deformation is expected generally in the region 650 ± 80 cm^{-1} (Roeges, 1994) and in the present case it is assigned at 599 and 585 cm^{-1} (DFT) for **3** and **2**, respectively.

The CH_3 stretching modes of the title compounds, **3** and **2** are assigned at 2920 cm^{-1} (IR), 2970, 2925 cm^{-1} (Raman), 3016, 2962, 2916 cm^{-1} (DFT) and at 2957, 2915 cm^{-1} (IR), 3005, 2960, 2916 cm^{-1} (Raman), 3013, 2957, 2913 cm^{-1} (DFT) as expected in literature (Roeges, 1994; Colthup et al., 1990). The bending modes of the methyl groups are observed at 1440, 1026 cm^{-1} (IR), 1370, 1024, 1000 cm^{-1} (Raman), 1448, 1442, 1368, 1024, 996 cm^{-1} (DFT) for **3** and at 1430, 1364, 1015 cm^{-1} (IR), 1435, 1358, 1025 cm^{-1} (Raman), 1442, 1432, 1366, 1023, 979 cm^{-1} (DFT) for **2** Roeges, 1994; Colthup et al., 1990.

In poly substituted benzenes, the aromatic CH stretching modes (Varsanyi, 1974) absorb weakly to moderately between 3000 and 3120 cm^{-1} and in the present case, the modes at 3090 (PhI) and 3081, 3056 cm^{-1} (PhII) (DFT) are assigned the CH stretching modes of **3** and 3071, 3057, 3042 cm^{-1} (PhI) and 3058, 3039 cm^{-1} (PhII) (DFT) for **2** Mary et al., 2015. Experimentally these modes are observed at 3060 cm^{-1} (IR), 3094, 3079, 3048 cm^{-1} (Raman) and at 3055 cm^{-1} (IR), 3055, 3058, 3033 cm^{-1} (Raman) for **3** and **2**, respectively. For **3** and **2**, the ring stretching modes are assigned at 1592, 1539, 1377, 1372, 1324 cm^{-1} for PhI, 1577, 1474, 1324, 1302, 913 cm^{-1} for PhII and at 1607, 1548, 1489, 1377, 1343, 1030 cm^{-1} for PhI, 1581, 1457, 1304, 1199, 893 cm^{-1} for PhII, theoretically (Roeges, 1994). Experimentally these ring stretching modes are observed at 1593, 1572, 1480, 1374, 1321 cm^{-1} in the IR spectrum, 1601, 1573, 1472, 1330, 1306 cm^{-1} in the Raman spectrum for **3** and at 1605, 1578, 1460, 1380, 1310, 1205, 1029 cm^{-1} in the IR spectrum, 1610, 1586, 1546, 1478, 1379, 1340, 1196, 889 cm^{-1} in the Raman spectrum for **2**. The ring breathing mode for poly substituted benzene ring is reported at 1006 cm^{-1} in the IR spectrum and at 998 cm^{-1} theoretically (Panicker et al., 2007) and at 1003 cm^{-1} theoretically (Mary et al., 2015). In the present case, the bands at 1119, 1065 cm^{-1} (IR), 1182 cm^{-1} (Raman), 1179, 1127, 1072, cm^{-1} (DFT) and 1154, 1078, 1029 cm^{-1} (IR), 1148, 1060 cm^{-1} (Raman), 1253, 1150, 1122, 1071, 1030 cm^{-1} (DFT) are assigned as the in-plane and out-of-plane CH deformations of the title compounds, **3** and **2**, respectively. The out-of-plane CH deformation modes are assigned at 957, 835, 810 cm^{-1} (IR), 950, 845, 803 cm^{-1} (DFT) for **3** and at 855, 799, 725 cm^{-1} (IR), 919, 855, 810, 727 cm^{-1} (Raman), 945, 924, 851, 808, 727 cm^{-1} (DFT) for **2**, respectively.

According to literature data (Socrates, 2001), for tetra-substituted benzenes, a strong band is seen in 850–840 cm^{-1} due to out-of-plane CH deformation and in the present case this mode appears at 855 and 835 cm^{-1}. Quinoline ring stretching modes at 1563 cm^{-1} in IR spectrum (Ulahannan et al., 2015), 1560 cm^{-1} in Raman spectrum and 1568 cm^{-1} theoretically (C═C stretching mode), 1500 cm^{-1} in the Raman spectrum and 1527 cm^{-1} theoretically (C═N stretching), 1281 cm^{-1} in the IR spectrum, 1285 cm^{-1} in Raman spectrum and 1285 cm^{-1} theoretically (C—N stretching), 1476 cm^{-1} in IR, 1205 cm^{-1} in Raman, 1204 and 1474 cm^{-1} theoretically (C—C stretching modes).

According to literature the C—Cl stretching mode is obtained in the wide region 850–550 cm^{-1} and the PED analysis gives a PED of 39 and 40% with IR intensities, 34.85 and 17.00, with Raman activities 1.09 and 0.66 for the C—Cl stretching modes with the theoretical values at 742 and 671 cm^{-1} which is in agreement with the reported literature (Parveen et al., 2016) and experimentally bands are observed 735, 674 cm^{-1} in the IR spectrum and at 740, 675 cm^{-1} in the Raman spectrum.

4.2. Frontier molecular orbital analysis and charge transfer

In order to understand global stability and reactive properties of investigated compounds we have analyzed frontier molecular orbitals. Namely, the highest occupied molecular orbital (HOMO) and lowest unoccupied molecular orbital (LUMO) are the main molecular orbitals that take part in reactions with other molecular structures. Distribution of HOMO and LUMO provides important insight into the reactive properties of organic molecules. Visualization presented in Fig. 2 indicates that HOMO is delocalized over the entire molecule and LUMO is delocalized over the entire molecule except CH_3 group for molecule **2**, while in the case of **3** HOMO is delocalized over the entire molecule except CH_3 while LUMO is delocalized over the entire molecule.

Using information on the energies of HOMO and LUMO, useful and frequently used quantum-molecular descriptors such as the ionization energy and electron affinity can be calculated according to the following simple relations: $I = -E_{HOMO}$, $A = -E_{LUMO}$, $\eta = (-E_{HOMO} + E_{LUMO})/2$ and $\mu = (E_{HOMO} + E_{LUMO})/2$ Fukui, 1982. Parr and Pearson (1983) proposed the global electrophilicity power of a ligand as $\omega = \mu^2/2\eta$. For the title compounds, energy difference between HOMO and LUMO, HOMO-LUMO gap, are equal to 4.81 eV, 4.27 eV and 4.08 eV for **1**, **2** and **3**, respectively, which are relatively high values indicating significant stability of these potentially pharmaceutical molecules.

Ionization potential, I, and electron affinity, A, are calculated to be 8.475 eV, 7.346 eV and 5.218, 5.032 eV for **2** and **3**, respectively. The values of HOMO-LUMO gap and global

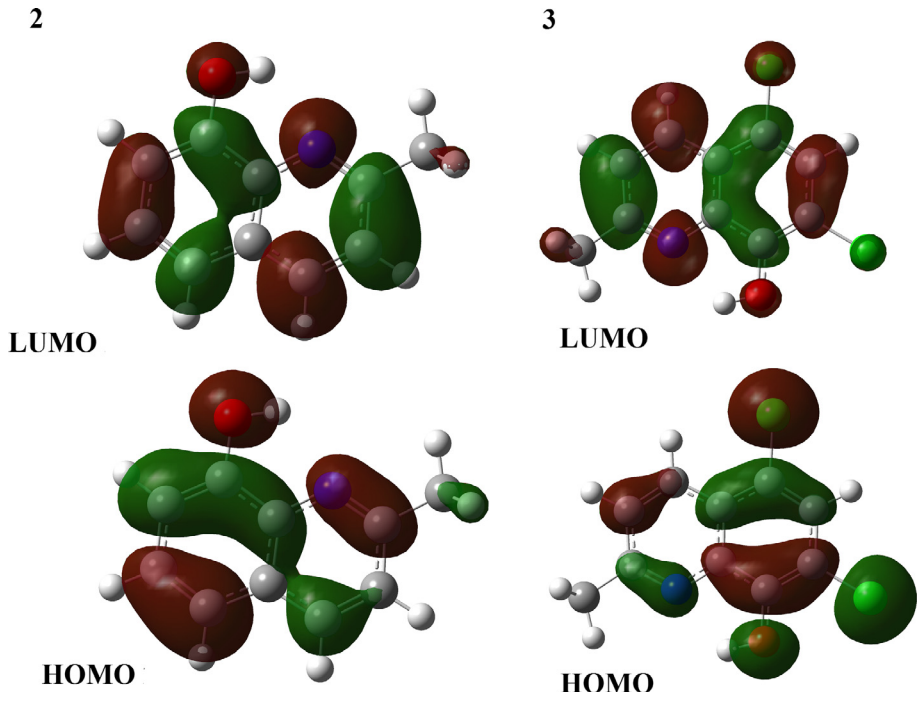

Fig. 2 Frontier molecular orbitals of quinoline derivatives 8-hydroy-2-methyl quinoline (**2**) and 5,7-dichloro-8-hydroy-2-methyl quinoline (**3**).

hardness (η = 1.628 for **2** and 1.157 eV for **3**) are almost the same as in the case of other similar derivatives that we have previously investigated (Ulahannan et al., 2015; Luque et al., 2000). There are significant differences in the values of chemical potential and global electrophilicity. Also, the calculated electrophilicity of the **2** and **3** molecules are 14.398 and 16.553 eV, which is significantly lower than the value of electrophilicity of derivative in literatures data (Ulahannan et al., 2015; Luque et al., 2000), with the values of 28.29 and 24.40 eV, meaning that the title molecules are much more stable.

It is known that HOMO-LUMO gap as a stability descriptor sometimes has certain limitations (La Porta et al., 2011; Lee et al., 2015; da Silva et al., 2006). Therefore, it is always useful to rely on some additional stability descriptors as well. In this work, using the concept of nucleus independent chemical shifts (NICS) approach recommended by Schleyer et al. (1996), we have also checked the aromaticity in order to explain the higher stability of **2** comparing with **3**. Particularly, we have observed the NICSzz parameter, which is recommended as better aromaticity criterion than NICS (Corminboeuf et al., 2004). NICSzz values of **2** and **3** have been calculated to be −77.38 and −23.66 ppm, respectively, indicating that **2** is more stable than **3**, which is in agreement with results related to HOMO-LUMO gaps. However, NICSzz parameter for **1** doesn't follow the trend as obtained by HOMO-LUMO gap, which is expected due to the fact that **1** and **3** differ significantly, because benzene ring in the case of **3** is modified at three positions comparing to the benzene ring of **1**.

Results presented in Fig. 2 indicate that charge transfer occurs within the whole molecules, since frontier molecular orbitals are distributed over the whole molecules. Since charge transfer studies can be also used for investigation of stability, we were motivated to try to correlate the trends related to HOMO-LUMO gap with charge transfer that occurs as a consequence of the first (lowest energy) excitation. In order to do so, we have used the a Multiwfn (Lu and Chen, 2012a, 2012b; Tian and Feiwu, 2011; Meng Xiao, 2015) program to investigate the charge transfer due to the excitation by examining electron density variation and $C_{+/-}$ functions (Le Bahers et al., 2011), which were visualized using the VMD program (Humphrey et al., 1996; Stone and Gu, 2001; Eargle et al., 2006; Frishman and Argos, 1995; Varshney et al., 1994; Sanner et al., 1995; Sharma et al., 2000). The concept behind the $C_{+/-}$ functions is very useful, as it allows one to quantify the amount of charge transfer by calculation of charge transfer length (CT length), which is defined as a distance between the barycenters of C_+ and C_- functions. Fig. 3 contains visualized $C_{+/-}$ functions with indicated CT lengths, with green color corresponding to the C_+ and blue color corresponding to the C_-. In order to study the charge transfer due to the excitation, it was necessary to perform single point time-dependent DFT (TD-DFT) calculations, which were done with CAM-B3LYP (Yanai et al., 2004) functional and 6-31 + G(d,p) level of theory, including the solvent effects of acetonitrile.

Results provided in Fig. 3 indicate that CT length, and thus the charge transfer, increases from **1** to **3** as a consequence of the lowest energy excitation, following the same trend HOMO-LUMO gaps. As the amount of charge transfer according to C functions increase, it can be concluded that the larger part of molecule is excited, which decreases the stability from **1** to **3**. Value of CT length in the case of **1** (0.98 Å) indicates rather small charge transfer, thanks to which that excitation can be characterized as locally excited (LE) type. On the other side, CT lengths of quinoline derivatives **2** and **3** are two times larger than in the case of **1**, indicating much higher charge transfer, thanks to which those excitations could be characterized as

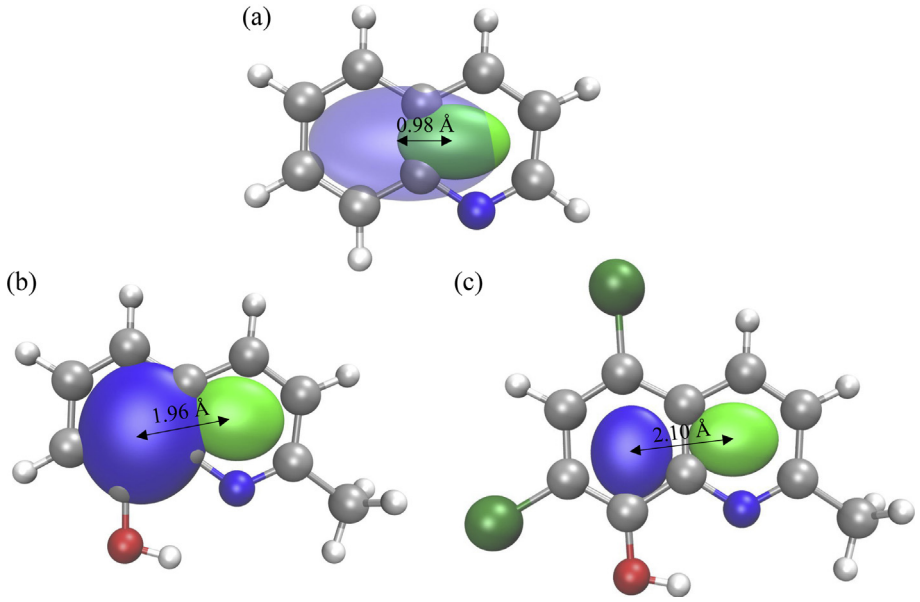

Fig. 3 $C_{+/-}$ functions of (a) **1**, (b) **2** and (c) **3**, with indicated CT lengths.

charge transfer (CT) type. Additionally, the transferred charge of positive and negative parts was calculated to be 0.381, 0.568 and 0.576 for **1**, **2** and **3**, respectively. The difference in HOMO-LUMO gap between the **1** and **2** is much higher than between the **2** and **3**, which is in accordance with the results obtained for CT length and transferred charge.

4.3. Molecular electrostatic potential

In this work MEP values have been mapped to electron density surface in order to obtain important information on charge density. Knowing charge density within molecule is of great importance for the determination of reactive sites prone to electrophilic and nucleophilic sites (Politzer et al., 1991; Murray and Sen, 1996). The interactions between the molecules and the physiochemical property relationships can be studied by using the MEP map (Seminario, 1996; Murray et al., 1990). The different values of the electrostatic potential at the MEP surface are given by different colors with potential values increases in the order red < orange < yellow < green < blue. The negative (red and yellow) regions of MEP surface (Fig. 4) were related to electrophilic reactivity while the positive (blue) regions to nucleophilic reactivity. For *2* the negative regions are over the ring PhI and oxygen atom while for **3**, the negative regions over the oxygen atom.

4.4. ALIE surface, Fukui functions and noncovalent interactions

In this work molecule sites potentially prone to electrophilic attacks have been determined by ALIE surfaces as well. ALIE surface of pristine quinoline has been compared with surfaces of the two quinoline derivatives, in order to determine the influence of structural changes. In general, for determination of molecule sites prone to electrophilic attacks it is better to employ ALIE surfaces than MEP surface. ALIE surfaces straightforwardly indicate molecule areas where electrons are least tightly bound (Politzer et al., 1998, 2010; Bulat et al., 2010; Michalak et al., 1999). ALIE surfaces of pristine quinoline (**1**), its derivative with methyl and OH groups (**2**) and its derivative with methyl, OH groups and chlorine atoms (**3**) are presented in Fig. 5.

Results presented in Fig. 5 indicate that sensitivity of quinoline towards electrophilic attacks reduces by the aforementioned modifications, as the lowest ALIE values increase for ~14 and 33 kcal/mol in cases of **2** and **3**, respectively. These results indicate that the lowest amount of energy required for

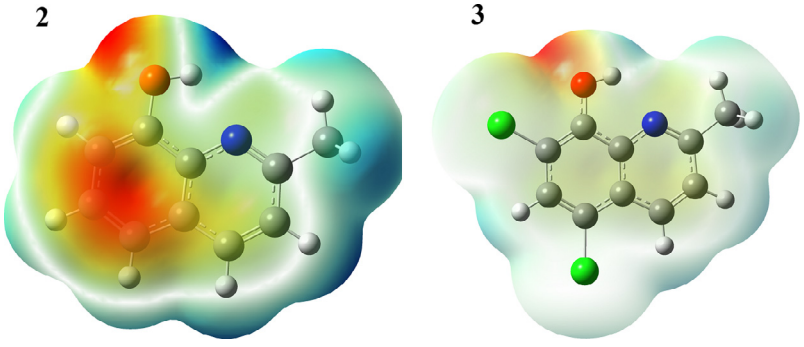

Fig. 4 MEP surfaces of 8-hydroy-2-methyl quinoline (**2**) and 5,7-dichloro-8-hydroy-2-methyl quinoline (**3**).

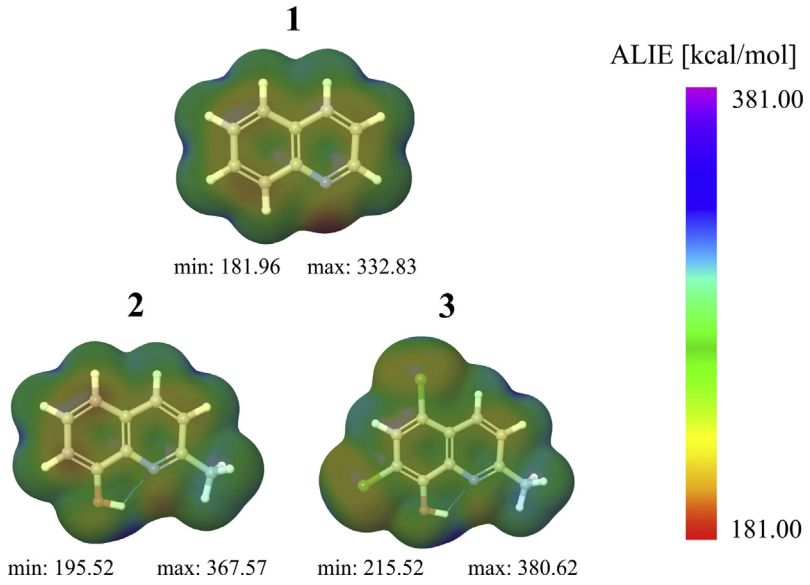

Fig. 5 Comparison of ALIE surfaces of quinoline and its derivatives.

removal of electron increase. On the other side the maximal ALIE values in case of **2** and **3** increase for ~35 and 48 kcal/mol comparing to **1**, indicating that electrons are much tighter bonded in the case of **2** and **3** derivatives thus favoring the nucleophilic attacks. Analysis of electron density between atoms indicates formation of one intra-molecular noncovalent interaction in the case of new quinoline derivatives. Noncovalent interactions are formed between hydrogen atom belonging to OH group and nitrogen atom, with corresponding strength of −0.025 and −0.026 electron/bohr^3, for **2** and **3** respectively.

The concept of Fukui functions is well established and it is particularly useful for determination of local reactivity properties when a set of similar molecules is analyzed. Values of Fukui functions in this work have been mapped to the electron density surface and the applied equations:

$$f^{+} = \frac{(\rho^{N+\delta}(r) - \rho^{N}(r))}{\delta}, \quad f^{-} = \frac{(\rho^{N-\delta}(r) - \rho^{N}(r))}{\delta} \tag{1}$$

where N stands for the number of electrons in reference state of the molecule, while δ stands for the fraction of electron which default value is set to be 0.01 (Andersson et al., 2014). Fukui functions of molecules investigated in this work are presented in Fig. 6, with purple and red designating positive and negative colors, respectively.

Positive (purple) color in Fig. 6a shows where electron density had been increased after the addition of charge, while negative (red) color in Fig. 6b shows areas where electron density had been decreased after the removal of charge. In Fig. 6a, in the case of Fukui f^{+} function, it can be seen that pristine quinoline (**1**) has three molecule sites with positive values of Fukui functions, indicating the areas where electron density increases after the addition of charge. However, this surface area with positive color decreases subsequently going from **1** to **3**, remaining within the nitrogen containing ring. In Fig. 6b, in the case of Fukui f^{-} function, it can be also seen that negative Fukui values are located between two rings, however as a consequence of structure modification with methyl and OH group, structure **2**, negative color moves to the methyl group, designating this molecule site as possibly important

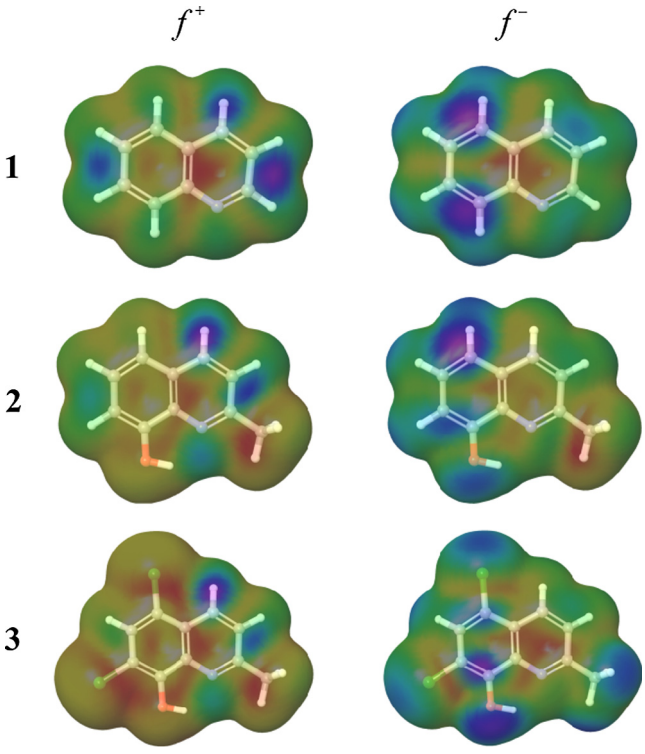

Fig. 6 Fukui functions of quinoline and its derivatives.

reactivity site. In the case of **3**, surface areas with negative color are located within nitrogen containing ring and in the near vicinity of chlorine atoms, designating them also as possibly important reactive sites.

4.5. Nonlinear optical properties

Quantum chemical calculations are widely used for the description of the relation between the electronic structure of systems and its nonlinear response (Burland et al., 1994).

Nonlinear optics deals with the interaction of electromagnetic fields in various materials to generate new electromagnetic fields, altered in wavenumber and other physical properties of the molecular systems (Shen, 1984). The calculated polarizability of **2** and **3** are 1.935×10^{-23} and 2.372×10^{-23} esu and 1.180 and 1.446 times of **1** (1.64×10^{-23}). The dipole moments of **2** and **3** are respectively, 2.99 and 4.2229 Debye and 1.373 and 1.933 times that of **1** (2.1842). The first order hyperpolarizabilities are 3.241×10^{-30} and 6.300×10^{-30} for **2** and **3** which are comparable with the reported values of similar derivatives (Ulahannan et al., 2015) and these values are 24.93 and 48.46 times that of the standard NLO material urea (Adant et al., 2004) while the first order hyperpolarizability of **1** is 0.982×10^{-30} esu. The reported values of first hyperpolarizability of similar derivatives are 5.37×10^{-30} (Ulahannan et al., 2015) and 16.9×10^{-30} (Ulahannan et al., 2015). The theoretically predicted second order hyperpolarizabilites are -4.403×10^{-37} esu for **2** and -8.040×10^{-37} esu for **3** and the reported values are -28.33×10^{-37} esu (Ulahannan et al., 2015), -21.14×10^{-37} esu (Luque et al., 2000). The second order hyperpolarizability of **2** and **3** are 1.56 and 2.85 times that of **1** (-2.825×10^{-37} esu). Hence the title compounds and its derivatives are good objects for further studies of nonlinear optical properties. The calculated C—N distances (C_4—N_7 = 1.3608, 1.3594 and C_8—N_7 = 1.3190, 1.3191) in the molecular structures of the title compounds are intermediate between those of single and double bond distances of C—N bond and hence, the calculated data suggests an extended π-electron delocalization of the quinoline moiety, which are responsible for the nonlinearity of the molecules (Tian et al., 2002).

4.6. Natural bond orbital analysis

The NBO calculations were performed using NBO 3.1 program (Glendening et al., 2003) as implemented in the Gaussian09 package at the DFT/B3LYP level in order to understand various second-order interactions. It also provides an efficient method for studying interesting features of molecular structure and serves as a convenient basis for the investigation of charge transfer or conjugative interactions in molecular system (Weinhold and Landis, 2001). The second order Fock matrix was carried out to evaluate the donor–acceptor interactions in the NBO analysis.For each donor (i) and acceptor (j) the stabilization energy (E2) associated with the delocalization i → j is determined as:

$$E(2) = \Delta E_{ij} = q_i \frac{(F_{i,j})^2}{(E_j - E_i)},$$

where q_i is the donor orbital occupancy, E_i, E_j are diagonal elements (orbital energies) and $F(_{i,\ j})$ is the off-diagonal NBO Fock matrix clement. The important interactions are tabulated in Tables S2 and S3 of the supplementary materials. The larger the $E(2)$ value is, the more intensive is the interaction between electron donors and electron acceptors.

The strong interaction $n_2O_{11} \rightarrow \pi^*(C_2{-}C_3)$ in both the compounds **2** and **3** have the highest $E(2)$ values 33.62, 37.21 kcal/mol respectively. The larger the $E(2)$ value, the intensive is the interaction between electron donors and electron acceptors. The strong interaction occur in both the compounds are $\pi(C_2{-}C_3) \rightarrow \pi^*(C_1{-}C_6)$ and the energy value gives the donor-acceptor interaction. Table S2 gives the occupancy of electrons and p-character (Reed et al., 1988) in significant NBO natural atomic hybrid orbitals. The 100% p-character was observed in π bonding of C_1—C_6, C_2—C_3 and the lone pairs of n_2 Cl_{12}, n_3Cl_{12}, n_3Cl_{13}, n_2O_{11} in **3**. The high p-character value of **2** is due to π bonding of C_2—C_3 and a lone pair of n_2O_{11}.

4.7. Reactive and degradation properties based on autoxidation and hydrolysis

Molecules investigated in the present study could be of importance for the development of new pharmaceutical products. In the case of this class of molecules, computational studies DFT calculations and MD simulations are precious tools for predic-

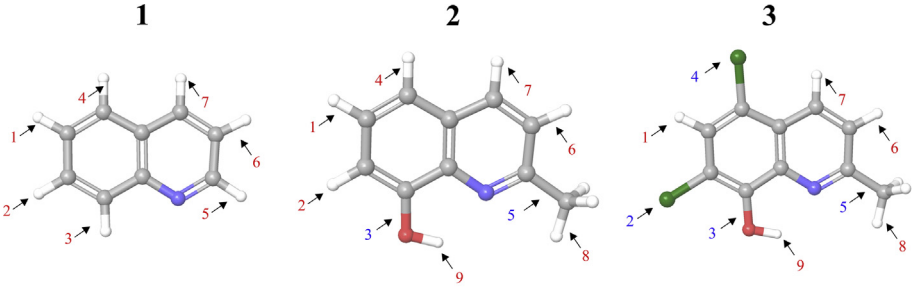

Bond number	1	2	3
1	117.67	117.24	120.29
2	117.37	119.72	90.77
3	119.58	119.45	119.73
4	117.06	118.24	90.08
5	110.19	99.22	100.15
6	117.90	117.45	117.95
7	116.48	116.69	118.01
8	–	94.33	94.75
9	–	94.52	92.52

Fig. 7 BDE values of all single acyclic bonds for quinoline and its derivatives.

tion of reactive properties and sensitivity towards important mechanisms (Ren et al., 2013; Ai and Liu, 2014; Sang-aroon et al., 2013; Kieffer et al., 2010). In the case of DFT calculations it is particularly useful to calculated BDE for hydrogen abstraction due to the correlation with oxidation reactions (Hovorka and Schöneich, 2001; Connors et al., 1986; Johnson and Gu, 1988). On the other side RDF calculated after MD simulations provide information about the stability in water and determine which atoms of target molecule have the most pronounced interactions with water molecules.

If the BDEs for hydrogen abstraction take values somewhere between 70 and 85 kcal/mol (Wright et al., 2009; Gryn'ova et al., 2011), then target molecule is possibly sensitive towards the autoxidation. Also, one should pay attention to the BDE values between 85 and 90 kcal/mol as well, as they could also be of importance for the aforementioned mechanism (Gryn'ova et al., 2011). BDE values for hydrogen abstraction that are lower than 70 kcal/mol are not appropriate for autoxidation (Lienard et al., 2015; Burland et al., 1994; Wright et al., 2009). BDE values for all single acyclic bonds for molecules investigated in this work are presented in Fig. 7. Red color designates BDE for hydrogen abstraction, while blue color indicates BDE for the rest of the single acyclic bonds.

BDE values for hydrogen abstraction of **1** emphasize great stability towards autoxidation. According to BDE quinolone is characterized by great stability in open air or in the presence of oxygen. Molecules **2** and **3**, are also stable towards autoxidation according to the results presented in Fig. 7, however substantial decrease in the BDE values for hydrogen abstraction are observable, especially in the case of **3** for which BDE for hydrogen abstraction almost fall in the critical interval between 70 and 90 kcal/mol. This indicates that further modifications might lead to the quinoline derivatives that are prone to autoxidation.

In this work we have also investigated stability of quinoline derivatives, **2** and **3**, in the water and compared it with pristine quinoline. In order to do so we have calculated interaction energies with the solvent and radial distribution functions (RDF) after MD simulations. The results are presented in Fig. 8.

Results of MD simulations clearly indicate that the modifications of quinoline with OH, methyl groups and chlorine atoms lead to the improved interactions with water. Interaction energy with water in the case of **1** is ~−25 kcal/mol and it significantly increase subsequently for ~−5 kcal/mol (20%) in the cases of **2** and **3**, respectively (Fig. 8). RDFs also confirm the fact that interactions with water molecules are much more pronounced in the cases of **2** and **3**, comparing to **1**. Namely, in the case of **1** only four atoms have relatively pronounced interactions with water molecules and all maximal g(r) values are located significantly above 2 Å. Introduction of OH group in the cases of **2** and **3** significantly improve the interactivity with water as hydrogen atom of OH group has very pronounced interactions with water, characterized by sharp g(r) profile with two distinct peaks and with the first maximal g(r) value located below 2 Å. In the case of **2** and **3**, oxygen atoms also have RDFs indicating relatively significant interactions with water molecules. In the case of **3** chlorine atoms also have sharp g (r) profiles indicating their importance when it comes to the interactions with water. Namely, RDFs of two chlorine atoms are practically identical, with maximal g(r) values located at around 3.5 Å. Introduction of methyl group also turned out to be important for the improvement of interactions with water molecules, since in the cases of both **2** and **3** carbon atom of methyl group had the highest maximal g(r) value of around 1.5, located at the distance of around 3.7 Å.

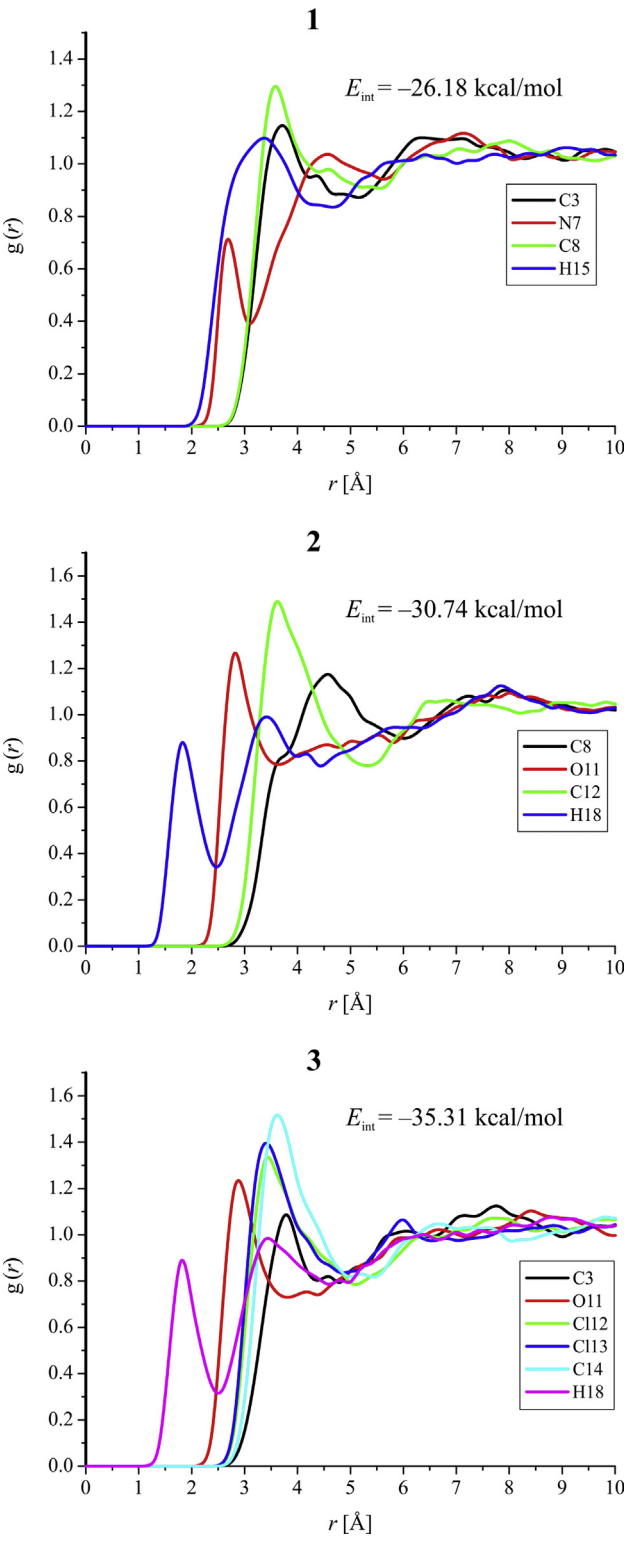

Fig. 8 RDFs of quinoline and its derivatives.

MD simulations with explicit involvement of solvent molecules enabled us to use the concept of atoms in molecules (AIM) in order to investigate in more details the interactions between water from one side and molecules **1**, **2** and **3** from the other side. Namely, by analyzing electron density one can identify the points characterized by zero electron density gradient. These points are the so called critical points and in general there are four types of critical points. In order to determine whether bonding interactions exist between the atoms that are not covalently bound, the most important are the bond critical points, which are characterized by minimal electron density at some point along the line connecting two atoms, while in the same time electron density is maximal in both directions perpendicular to the bond.

From the last frame of MD simulation we have extracted molecules **1**, **2** or **3**, as surrounded by water molecules in radius of 3 Å and run a single point energy calculation with the command to perform an analysis of electron density and search for noncovalent interactions at DFT/B3LYP/6-31 + G(d,p) level of theory. The obtained results have been presented in Fig. 9.

In order to get a clear view, water molecules in Fig. 9 have been visualized in wire representation. All bond critical paths between observed quinoline based molecule and water molecule have been presented as dashed line. Bond critical points have been visualized as dummy atoms only for atoms with significant interactions according to RDFs, for which strength of interaction is expressed in terms of density (electron/bohr^3). Results presented in Fig. 9 confirm the results obtained by MD simulations. Namely, the magnitude of E_{int} increases subsequently from **1** to **3** and the same trend can be observed if the number and strengths of detected noncovalent interactions are analyzed.

Namely, according to Fig. 8, **1** has the lowest E_{int} due to the absence of OH group, although nitrogen atom of **1** has strong noncovalent interaction with water molecule (Fig. 9a) with corresponding strength of −0.055 electron/bohr^3. Fig. 9b and c explain why **3** has higher E_{int} than **2**. Namely, in the case of **3**, oxygen atom of OH group is involved in one additional noncovalent interaction which contributes to the E_{int}, comparing with **2**. Besides, as it can be seen in Fig. 9, the strengths of the most important noncovalent interactions in case of **3** are significantly higher in magnitude than in the case of **2**, which explain the observed trend concerning the E_{int}.

4.8. Drug likeness

According to the detailed study of more than 2000 drugs Lipinski et al. (1997), Lipinski (2004) defined a famous rule of five, often called Lipinski's rule of five or Pfizer's rule of five. This rule serves as an indicator to what extent some compound can be considered as membrane permeable and absorbed in the

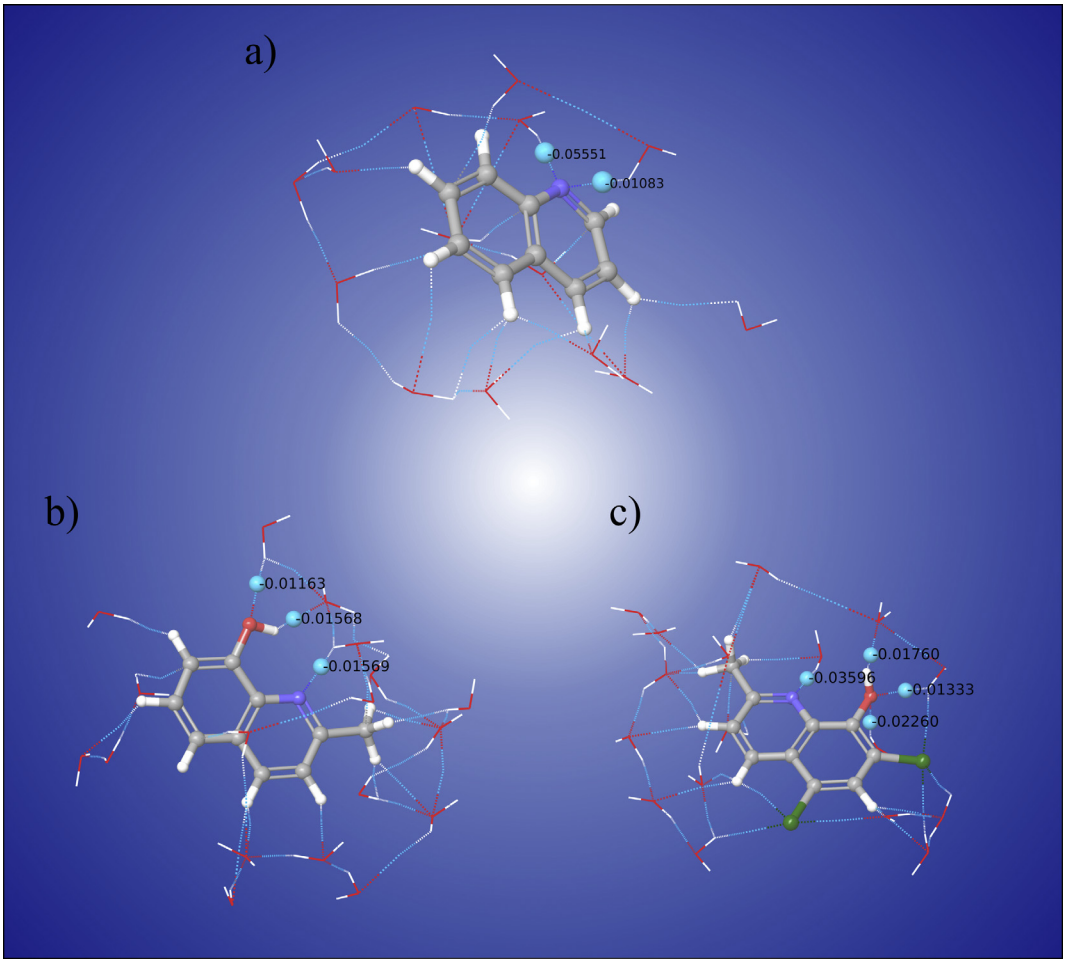

Fig. 9 Analysis of noncovalent interactions between water molecules and (a) **1**, and its derivatives (b) **2** and (c) **3**.

Table 1 Relevant drug likeness parameters.

Descriptor	Value		Desired range	
	2	**3**	Rule of five	Rule of three
Hydrogen Bond Donor (HBD)	1	1	< 5	< 3
Hydrogen Bond Acceptor (HBA)	2	2	< 10	< 3
Mass	159.189	228.079	< 500	< 300
AlogP	2.032	3.360	< 5	< 3
Polar surface area (PSA) [Å^2]	33.120	33.120	< 140	< 140
Molar refractivity	46.573	56.183	40–130	40–130
Number of rotatable bonds	0	0	< 10	< 3

human organism. What is even more important all of these parameters can be inexpensively calculated by various molecular modeling packages. In this work we used Maestro to calculate relevant drug likeness parameters provided in Table 1.

Moderately lipophilic property is necessary in order for some molecule to be considered as a prospective drug candidate and this property is characterized by octanol/water partition coefficient values lower than 5. In this work AlogP (Ghose et al., 1998; Ghose and Crippen, 1987, 1986; Viswanadhan et al., 1989; Ghose et al., 1988) value has been calculated to be 2.032 and 3.360 for quinoline derivatives **2** and **3**, while pristine quinoline **1** has an AlogP value of 2.016. These AlogP values emphasize the potential of new quinoline derivatives investigated in this work. HBD and HBA are also important factors for drug likeness and these values should lower than 5 and 10, respectively. Due to the size of molecules investigated in this study these conditions are easily fulfilled. Same applies for the conditions related molecule mass and number of rotatable bonds, which are also easily fulfilled. Veber et al. (2002) introduced the condition that number of rotatable bonds should be lower than 10. Ghose et al. (1999) recommended values of molar refractivity and polar surface area that prospective drug candidates should have. According to Ghose et al. molar refractivity should be in the range of 40–130, while polar surface area should be lower than 140 Å^2. Inspection of results provided in Table 1 clearly shows that these conditions are also fulfilled by quinoline derivatives **2** and **3**. These even more harsh criteria are also fulfilled by quinoline derivatives presented in this study. Finally, it is very important to mention the very demanding "rule of three", defined by Congreve et al. (2003), according to which logP value, HBD, HBA and number of rotatable bonds all should be lower than 3, while mass should be lower than 300 u. Another inspection of Table 1 clearly indicates that these very harsh conditions are completely fulfilled by quinoline derivative **2**, which makes it a prospective candidate for drug.

4.9. Molecular docking studies

The emergence of drug-resistant malaria parasites continues to hamper efforts to control the lethal disease malaria. Dihydroorotate dehydrogenase has recently been validated as a new target for the treatment of malaria, and a selective inhibitor (DSM265) of the Plasmodium enzyme is currently in clinical development (Phillips et al., 2016). Using the PASS (Prediction of Activity Spectra) (Lagunin et al., 2000) analysis predicted activities of **2** and **3** have been tabulated in Table 2.

Results in Table 2 suggested that dehydrogenase inhibitor with probability to be active (Pa) value higher than 0.9 should be used as a target for docking study. Quinoline-based drug (Chloroquine CQ) is widely used for the prevention and treatment of malaria. Quinoline-containing antimalarial drugs, such as chloroquine, quinine and mefloquine, are mainstays

Table 2 PASS prediction for the activity spectrum of the compounds 2 and 3. Pa represents probability to be active and Pi represents probability to be inactive.

8-Hydroy-2-methyl quinoline **(2)**			5,7-Dichloro-8-hydroy-2-methyl quinoline **(3)**		
Pa	Pi	Activity	Pa	Pi	Activity
0.961	0.001	Corticosteroid side-chain-isomerase inhibitor	0.934	0.003	Antiseborrheic
0.952	0.001	Amine dehydrogenase inhibitor	0.903	0.004	Taurine dehydrogenase inhibitor
0.948	0.002	Taurine dehydrogenase inhibitor	0.862	0.003	Corticosteroid side-chain-isomerase inhibitor
0.933	0.002	Dehydro-L-gulonate decarboxylase inhibitor	0.859	0.003	Amine dehydrogenase inhibitor
0.922	0.002	Alkane 1-monooxygenase inhibitor	0.845	0.025	Membrane integrity agonist
0.920	0.002	Glutathione thiolesterase inhibitor	0.789	0.003	Antiprotozoal (Amoeba)
0.915	0.002	Laccase inhibitor	0.797	0.021	Chlordecone reductase inhibitor
0.908	0.009	Membrane integrity agonist	0.773	0.004	Antiseptic
0.888	0.004	Arylacetonitrilase inhibitor	0.763	0.014	Dehydro-L-gulonate decarboxylase inhibitor
0.885	0.004	Monodehydroascorbate reductase (NADH) inhibitor	0.752	0.005	Laccase inhibitor
0.889	0.010	Aspulvinonedimethylallyltr-ansferase inhibitor	0.751	0.007	Trans-acenaphthene-1.2-diol dehydrogenase inhibitor
0.880	0.002	Cysteaminedioxygenase inhibitor	0.768	0.044	Ubiquinol-cytochrome-c reductase inhibitor
0.880	0.002	UGT2B12 substrate			
0.879	0.005	Glucose oxidase inhibitor			

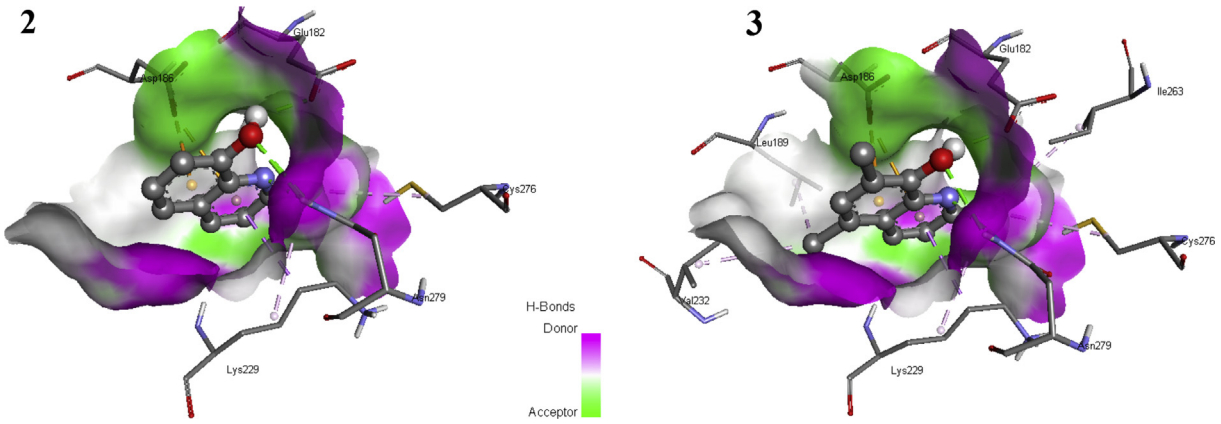

Fig. 10 The amino acids of dehydrogenase inhibitors interaction with the ligands **3** and **2** and the H-bond surfaces.

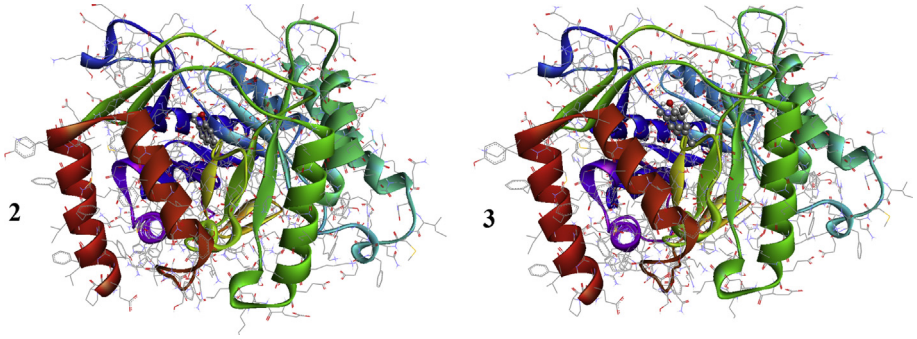

Fig. 11 The docked ligands **2** and **3** at the same catalytic site of the receptor dehydrogenase inhibitor.

Table 3 The binding affinity values of different poses of the compounds **2** and **3** predicted by AutodockVina.

8-Hydroy-2-methyl quinoline **(2)**				5,7-Dichloro-8-hydroy-2-methyl quinoline **(3)**			
Mode	Affinity [kcal/mol]	Distance from the best mode		Mode	Affinity [kcal/mol]	Distance from the best mode	
		RMSD l.b.	RMSD u.b.			RMSD l.b.	RMSD u.b.
1	−6.2	0.000	0.000	1	−6.9	0.000	0.000
2	−6.1	1.597	3.928	2	−6.0	2.046	4.062
3	−6.0	14.701	15.996	3	−5.7	19.521	21.453
4	−5.9	2.228	4.540	4	−5.7	11.683	13.174
5	−5.8	13.773	14.782	5	−5.4	11.900	14.068
6	−5.7	1.346	3.720	6	−5.3	18.770	20.31
7	−5.3	13.633	15.591	7	−5.2	13.450	15.452
8	−5.3	2.319	3.158	8	−5.1	19.090	20.742

of chemotherapy against malaria (Golden et al., 2015; Foley and Tilley, 1998). As the malaria parasites become increasingly resistant to the quinoline antimalarials, there is an urgent need to design new antimalarial drugs and number of modified quinolines and bisquinoline compounds show some promise in this regard.

All molecular docking calculations were performed on Auto Dock-Vina software (Trott and Olson, 2010) and as reported in literature (Ulahannan et al., 2015). The docking protocol predicted the same conformation as was present in the crystal structure with RMSD value well within the reliable range of 2 Å (Kramer et al., 1999). Amongst the docked conformations, one which binds well at the active site was analyzed for detailed interactions in Discovery Studio Visualizer 4.0 software. The ligand binds at the active site of the substrate by weak non-covalent interactions and these interactions are depicted in Fig. 10.

Amino acid Asn279 forms two H-bond with quinoline ring and OH group and Glu182 shows H-bond interaction with OH group of the docked ligand. Asp186 forms π-anion interaction with quinoline and phenyl rings and Lys229 forms π-sigma interaction with quinoline ring. Lys229, Ile263, Cys276forms

alkyl interactions with CH_3 group attached to the quinoline ring and Leu189, Val232 hold alkyl interaction with CH_3 group attached to phenyl ring in both the compounds. Snapshots of the molecular docking study have been presented Fig. 11, while binding affinity values of several detected binding modes have been summarized in Table 3.

According to the obtained results it was concluded that the docked ligands form a stable complex with dehydrogenase inhibitor (Fig. 11). For both quinoline derivatives eight representative binding modes have been detected with binding affinities ranging from −6.2 kcal/mol to −5.3 kcal/mol for quinoline derivative **2** and ranging from −6.9 kcal/mol to −5.1 kcal/mol for quinoline derivative **3**, Table 3. As it can be seen somewhat higher binding affinity has been calculated in the case of quinoline derivative **3**, while both of these molecules can be considered as a lead compounds for the development of new anti-malarial drugs.

5. Conclusion

Global reactivity of **1**, **2** and **3** has been investigated with the help of HOMO-LUMO gap, indicating that stability decrease from **1** to **3**. This trend has been successfully correlated with the CT length. Distances between carbon and nitrogen atoms take intermediate values with respect to single and double bond distances between carbon and nitrogen atoms, thus the results obtained for NLO properties indicate an extended π-electron delocalization of the quinoline moiety, thanks to which the nonlinearity of investigated molecules can be explained. Investigation of ALIE surfaces indicated that sensitivities of quinoline derivatives, **2** and **3**, towards electrophilic attacks are lower than in the case of pristine quinoline, but in the same time their sensitivity towards nucleophilic attacks is higher due to the much higher values of the maximal ALIE values. The investigated compounds are also characterized by formation of one strong intramolecular noncovalent interaction between hydrogen atom of OH group and nitrogen atom. Fukui functions also confirmed the results of ALIE surfaces and indicated a decrease of number of electrophilic and increase of number of nucleophilic molecule sites going from **1** to **3**. BDE for hydrogen abstraction of all molecules investigated in this study show stability towards autoxidation, however it is also evident that modifications led to the substantial decrease of BDE values, very close to the desired interval between 70 and 90 kcal/mol. Interaction energies with solvent and RDFs, obtained after MD simulations, indicate that the present quinoline derivatives have much more pronounced interactions with water molecules than pristine quinoline. Hydrogen atom of OH group was especially important for the interactions with water molecules with maximal g(r) value located below 2 Å. The importance of the OH group in terms of reactivity with water has been also illustrated by investigation of noncovalent interactions between quinoline derivatives and water molecules. For nitrogen atom of **1** it was found to have significant interactions with water molecules, however the presence of OH group in **2** and **3** enables several more noncovalent interactions which contribute to the higher interaction energy. The docked ligands form a stable complex with dehydrogenase inhibitor and these quinoline derivatives can be a lead compounds for developing new anti-malarial drug.

Acknowledgment

Part of this work has been performed thanks to the support received from Schrödinger Inc. Part of this study was conducted within the projects supported by the Ministry of Education, Science and Technological Development of Serbia, grant numbers OI 171039 and TR 34019.

Appendix A. Supplementary material

Supplementary data associated with this article can be found, in the online version, at http://dx.doi.org/10.1016/j.arabjc.2017.07.006.

References

Abramović, B., Kler, S., Šojić, D., Laušević, M., Radović, T., Vione, D., 2011. Photocatalytic degradation of metoprolol tartrate in suspensions of two TiO_2-based photocatalysts with different surface area, Identification of intermediates and proposal of degradation pathways. J. Hazard. Mater. 198, 123–132.

Adant, C., Dupuis, M., Bredas, J.L., 2004. Ab initio study of the nonlinear optical properties of urea, electron correlation and dispersion effects. Int. J. Quantum Chem. 56, 497–507.

Afzal, O., Kumar, S., Haider, M.R., Ali, M.R., Kumar, R., Jaggi, M., Bawa, S., 2015. A review on anticancer potential of bioactive heterocycle quinoline. Eur. J. Med. Chem. 97, 871–910.

Ai, L.-L., Liu, J.-Y., 2014. Mechanism of OH-initiated atmospheric oxidation of E/Z-CF3CF = CFCF3: a quantum mechanical study. J. Mol. Model. 20, 1–10.

Andersson, T., Broo, A., Evertsson, E., 2014. Prediction of drug candidates' sensitivity toward autoxidation: computational estimation of C-H dissociation energies of carbon-centered radicals. J. Pharm. Sci. 103, 1949–1955.

Armaković, S., Armaković, S.J., Šetrajčić, J.P., Šetrajčić, I.J., 2012. Active components of frequently used β-blockers from the aspect of computational study. J. Mol. Model. 18, 4491–4501.

Armaković, S.J., Armaković, S., Finčur, N.L., Šibul, F., Vione, D., Šetrajčić, J.P., Abramović, B., 2015. Influence of electron acceptors on the kinetics of metoprololphotocatalytic degradation in TiO_2 suspension. A combined experimental and theoretical study. RSC Adv. 5, 54589–54604.

Armaković, S., Armaković, S.J., Abramović, B.F., 2016. Theoretical investigation of loratadine reactivity in order to understand its degradation properties: DFT and MD study. J. Mol. Modl. 22, 240.

Armaković, S.J., Grujić-Brojčin, M., Šćepanović, M., Armaković, S., Golubović, A., Babić, B., Abramović, B.F., 2019. Efficiency of La-doped TiO_2 calcined at different temperatures in photocatalytic degradation of β-blockers. Arab. J. Chem. 12 (8), 5355–5369.

Bank, P.D., 1971. Protein Data Bank. Nat. New Biol. 233, 223.

Becke, A.D., 1993. Density-functional thermochemistry. III. The role of exact exchange. J. Chem. Phys. 98, 5648–5652.

Berendsen, H.J., Postma, J.P. van Gunsteren, W.F., Hermans, J., 1981. Interaction models for water in relation to protein hydration, in Intermolecular forces. Springer. pp. 331–342.

Berman, H.M., Westbrook, J., Feng, Z., Gilliland, G., Bhat, T.N., Weissig, H., Shindyalov, I.N., Bourne, P.E., 2000. The protein data bank. Nucleic Acids Res. 28, 235–242.

Berman, H., Henrick, K., Nakamura, H., 2003. Announcing the worldwide protein data bank. Nat. Struct. Mol. Biol. 10, 980.

Bernstein, F.C., Koetzle, T.F., Williams, G.J., Meyer, E.F., Brice, M. D., Rodgers, J.R., Kennard, O., Shimanouchi, T., Tasumi, M., 1977. The protein data bank. FEBS J. 80, 319–324.

Bernstein, F.C., Koetzle, T.F., Williams, G.J., Meyer, E.F., Brice, M. D., Rodgers, J.R., Kennard, O., Shimanouchi, T., Tasumi, M., 1978. The Protein Data Bank: a computer-based archival file for macromolecular structures. Arch. Biochem. Biophys. 185, 584–591.

Blessy, M., Patel, R.D., Prajapati, P.N., Agrawal, Y., 2014. Development of forced degradation and stability indicating studies of drugs – a review. J. Pharm. Anal. 4, 159–165.

Bochevarov, A.D., Harder, E., Hughes, T.F., Greenwood, J.R., Braden, D.A., Philipp, D.M., Rinaldo, D., Halls, M.D., Zhang, J., Friesner, R.A., 2013. Jaguar: a high performance quantum

chemistry software program with strengths in life and materials sciences. Int. J. Quantum Chem. 113, 2110–2142.
Bowers, K.J., Chow, E., Xu, H., Dror, R.O., Eastwood, M.P., Gregersen, B.A., Klepeis, J.L., Kolossvary, I., Moraes, M.A., Sacerdoti, F.D., 2006. Scalable algorithms for molecular dynamics simulations on commodity clusters. In: SC 2006 Conference, Proceedings of the ACM/IEEE. IEEE.
Bregović, V.B., Basarić, N., Mlinarić-Majerski, K., 2015. Anion binding with urea and thiourea derivatives. Coord. Chem. Rev. 295, 80–124.
Bulat, F.A., Toro-Labbé, A., Brinck, T., Murray, J.S., Politzer, P., 2010. Quantitative analysis of molecular surfaces: areas, volumes, electrostatic potentials and average local ionization energies. J. Mol. Model. 16, 1679–1691.
Burland, D.M., Miller, R.D., Walsh, C.A., 1994. Second order nonlinearity in poled poymer systems. Chem. Rev. 94, 31–75.
Calhoun, W., Carlson, R.P., Crossley, R., Datko, L.J., Dietrich, S., Heatherington, K., Marshall, L.A., Meade, P.J., Opalko, A., Shepherd, R.G., 1995. Synthesis and antiinflammatory activity of certain 5, 6, 7, 8-tetrahydroquinolines and related compounds. J. Med. Chem. 38, 1473–1481.
Četojević-Simin, D.D., Armaković, S.J., Šojić, D.V., Abramović, B. F., 2013. Toxicity assessment of metoprolol and its photodegradation mixtures obtained by using different type of TiO_2 catalysts in the mammalian cell lines. Sc. Total Environ. 463, 968–974.
Cho, C.S., Oh, B.H., Shim, S.C., 1999. Synthesis of quinolines by ruthenium-catalyzed heteroannulation of anilines with 3-amino-1-propanol. J. Heterocycl. Chem. 36, 1175–1178.
Colthup, N.B., Daly, L.H., Wiberly, S.E., 1990. Introduction to Infrared and Raman Spectroscopy. Academic Press, New York.
Congreve, M., Carr, R., Murray, C., Jhoti, H., 2003. A 'rule of three'for fragment-based lead discovery? Drug Discov. Today 8, 876–877.
Connors, K.A., Amidon, G.L., Stella, V.J., 1986. Chemical stability of pharmaceuticals: a handbook for pharmacists. John Wiley & Sons.
Corminboeuf, C., Heine, T., Seifert, G., von Ragué Schleyer, P., Weber, J., 2004. Induced magnetic fields in aromatic [n]-annulenes—interpretation of NICS tensor components. PCCP 6, 273–276.
Coutinho, K., Canuto, S., Zerner, M., 2000. A Monte Carlo-quantum mechanics study of the solvatochromic shifts of the lowest transition of benzene. J. Chem. Phys. 112, 9874–9880.
Crousse, B., Bégué, J.-P., Bonnet-Delpon, D., 1998. Synthesis of tetrahydroquinoline derivatives from α-CF 3-N-arylaldimine and vinyl ethers. Tetrahedron Lett. 39, 5765–5768.
da Rocha, E.P., Rodrigues, H.A., da Cunha, E.F.F., Ramalho, T.C., 2016. Probing kinetic and thermodynamic parameters as well as solvent and substituent effects on spectroscopic probes of 2-amino-1,4-naphthoquinone derivatives. Comput. Theor. Chem. 1096, 17–26.
da Silva, R.R., Ramalho, T.C., Santos, J.M., Figueroa-Villar, J.D., 2006. On the limits of highest-occupied molecular orbital driven reactions: the frontier effective-for-reaction molecular orbital concept. J. Phys. Chem. A 110, 1031–1040.
de Souza, G.L., de Oliveira, L.M., Vicari, R.G., Brown, A., 2016. A DFT investigation on the structural and antioxidant properties of new isolated interglycosidic O-(1 → 3) linkage flavonols. J. Mol. Model. 22, 1–9.
Dennington, R., Keith, T., Millam, J., 2009. GaussView, Version 5. Semichem Inc., Shawnee Mission KS.
Djeradi, H., Rahmouni, A., Cheriti, A., 2014. Antioxidant activity of flavonoids: a QSAR modeling using Fukui indices descriptors. J. Mol. Model. 20, 1–9.
Eargle, J., Wright, D., Luthey-Schulten, Z., 2006. Multiple alignment of protein structures and sequences for VMD. Bioinformatics 22, 504–506.
Foley, M., Tilley, L., 1998. Quinolineantimalarials: mechanisms of action and resistance and prospects for new agents. Pharmacol. Ther. 79, 55–87.
Foresman, J.B., 1996. In: Frisch, E. (Ed.), Exploring Chemistry with Electronic Structure Methods: a Guide to Using Gaussian, Pittsburg, PA.
Frisch, M.J., Trucks, G.W., Schlegel, H.B., Scuseria, G.E., Robb, M. A., Cheeseman, J.R., Scalmani, G., Barone, V., Mennucci, B., Petersson, G.A., Nakatsuji, H., Caricato, M., Li, X., Hratchian, H. P., Izmaylov, A.F., Bloino, J., Zheng, G., Sonnenberg, J.L., Hada, M., Ehara, M., Toyota, K., Fukuda, R., Hasegawa, J., Ishida, M., Nakajima, T., Honda, Y., Kitao, O., Nakai, H., Vreven, T., Montgomery, Jr., J.A., Peralta, J.E., Ogliaro, F., Bearpark, M., Heyd, J.J., Brothers, E., Kudin, K.N., Staroverov, V.N., Keith, T., Kobayashi, R., Normand, J., Raghavachari, K., Rendell, A., Burant, J.C., Iyengar, S.S., Tomasi, J., Cossi, M., Rega, N., Millam, J.M., Klene, M., Knox, J.E., Cross, J.B., Bakken, V., Adamo, C., Jaramillo, J., Gomperts, R., Stratmann, R.E., Yazyev, O., Austin, A.J., Cammi, R., Pomelli, C., Ochterski, J.W., Martin, R.L., Morokuma, K., Zakrzewski, V.G., Voth, G.A., Salvador, P., Dannenberg, J.J., Dapprich, S., Daniels, A.D., Farkas, O., Foresman, J.B., Ortiz, J.V., Cioslowski, J., Fox, D.J., 2010. Gaussian 09, Revision B.01, Gaussian Inc., Wallingford, CT.
Frishman, D., Argos, P., 1995. Knowledge-based protein secondary structure assignment. Proteins: Struct., Funct., Bioinf. 23, 566–579.
Fukui, K., 1982. Role of frontier orbitals in chemical reactions. Science 218, 747–754.
Ghose, A.K., Crippen, G.M., 1986. Atomic physicochemical parameters for three-dimensional structure-directed quantitative structure-activity relationships I. Partition coefficients as a measure of hydrophobicity. J. Comput. Chem. 7, 565–577.
Ghose, A.K., Crippen, G.M., 1987. Atomic physicochemical parameters for three-dimensional-structure-directed quantitative structure-activity relationships. 2. Modeling dispersive and hydrophobic interactions. J. Chem. Inform. Comput. Sci., 27, 21–35.
Ghose, A.K., Pritchett, A., Crippen, G.M., 1988. Atomic physicochemical parameters for three dimensional structure directed quantitative structure-activity relationships III: modeling hydrophobic interactions. J. Comput. Chem. 9, 80–90.
Ghose, A.K., Viswanadhan, V.N., Wendoloski, J.J., 1998. Prediction of hydrophobic (lipophilic) properties of small organic molecules using fragmental methods: an analysis of ALOGP and CLOGP methods. J. Phys. Chem. A 102, 3762–3772.
Ghose, A.K., Viswanadhan, V.N., Wendoloski, J.J., 1999. A knowledge-based approach in designing combinatorial or medicinal chemistry libraries for drug discovery. 1. A qualitative and quantitative characterization of known drug databases. J. Comput. Chem. 1, 55–68.
Giacoppo, J.d.O., Carregal, J.B., Junior, M.C., Cunha, E.F.d., Ramalho, T.C., 2017. Towards the understanding of tetrahydroquinolines action in Aedes aegypti: larvicide or adulticide? Molecular Simulation, 43, 121–133.
Glendening, E.D., Reed, A.E., Carpenter, J.E., Weinhold, F., 2003. NBO Version 3.1, Gaussian Inc., Pittsburgh, PA.
Golden, E.B., Cho, H.Y., Hofman, F.M., Louie, S.G., Schönthal, A. H., Chen, T.C., 2015. Quinoline-based antimalarial drugs: a novel class of autophagy inhibitors. Neurosurg Focus 38 (3), E12. http://dx.doi.org/10.3171/2014.12.FOCUS14748.
Gonçalves, M.A., Santos, L.S., Prata, D.M., Peixoto, F.C., Cunha, E.F., Ramalho, T.C., 2017. Optimal wavelet signal compression as an efficient alternative to investigate molecular dynamics simulations: application to thermal and solvent effects of MRI probes. Theor. Chem. Acc. 136, 15.
Gryn'ova, G., Hodgson, J.L., Coote, M.L., 2011. Revising the mechanism of polymer autoxidation. Org. Biomol. Chem. 9, 480–490.
Guo, L.-J., Wei, C.-X., Jia, J.-H., Zhao, L.-M., Quan, Z.-S., 2009. Design and synthesis of 5-alkoxy-[1, 2, 4] triazolo [4, 3-a] quinoline

derivatives with anticonvulsant activity. Eur. J. Med. Chem. 44, 954–958.
Guo, Z., Mohanty, U., Noehre, J., Sawyer, T.K., Sherman, W., Krilov, G., 2010. Probing the α-helical structural stability of stapled p53 peptides: molecular dynamics simulations and analysis. Chem. Biol. Drug Des. 75, 348–359.
Harder, E., Damm, W., Maple, J., Wu, C., Reboul, M., Xiang, J.Y., Wang, L., Lupyan, D., Dahlgren, M.K., Knight, J.L., 2015. OPLS3: a force field providing broad coverage of drug-like small molecules and proteins. J. Chem. Theor. Comput. 12, 281–296.
Hovorka, S.W., Schöneich, C., 2001. Oxidative degradation of pharmaceuticals: theory, mechanisms and inhibition. J. Pharm. Sci. 90, 253–269.
Huang, G., Wu, X., Xie, Y., Kong, F., Zhang, Z., Siu, G., Chu, P.K., 2005. Photoluminescence from 8-hydroxy quinoline aluminum embedded in porous anodic alumina membrane. Appl. Phys. Lett. 87, 151910.
Humphrey, W., Dalke, A., Schulten, K., 1996. VMD: visual molecular dynamics. J. Mol. Graph. 14, 33–38.
Hussain, H., Al-Harrasi, A., Al-Rawahi, A., Green, I.R., Gibbons, S., 2002. Fruitful decade for antileishmanial compounds from 2002 to late 2011. Chem. Rev. 114 (2014), 10369–10428.
Johnson, D., Gu, L., 1988. Autoxidation and antioxidants. Encycl. Pharm. Technol. 1, 415–449.
Johnson, E.R., Keinan, S., Mori-Sanchez, P., Contreras-Garcia, J., Cohen, A.J., Yang, W., 2010. Revealing noncovalent interactions. J. Am. Chem. Soc. 132, 6498–6506.
Jorgensen, W.L., Tirado-Rives, J., 1988. The OPLS [optimized potentials for liquid simulationspotential functions for proteins, energy minimizations for crystals of cyclic peptides and crambin. J. Am. Chem. Soc. 110, 1657–1666.
Jorgensen, W.L., Maxwell, D.S., Tirado-Rives, J., 1996. Development and testing of the OPLS all-atom force field on conformational energetics and properties of organic liquids. J. Am. Chem. Soc. 118, 11225–11236.
Khan, S.A., Asiri, A.M., Al-Thaqafy, S.H., Aidallah, H.M.F., El-Daly, S.A., 2014. Synthesis, characterization and spectroscopic behavior of novel 2-oxo-1,4-disubstituted-1,2,5,6-tetrahydrobenzo [h]quinoline-3-carbonitrile dyes. Spectrochim. Acta 133, 141–148.
Khavani, M., Izadyar, M., Jamsaz, A., 2017. DFT investigation of the kinetics and mechanism of the thermal decomposition of oxalic acid. Prog. React. Kinet. Mech. 42, 44–51.
Kieffer, J., Brémond, É., Lienard, P., Boccardi, G., 2010. In silico assessment of drug substances chemical stability. J. Mol. Struct. THEOCHEM 954, 75–79.
Kramer, B., Rarey, M., Lengauer, T., 1999. Evaluation of the FlexX incremental construction algorithm for protein ligand docking, PROTEINS: Struct. Funct. Genet. 37, 228–241.
Kumar, S., Bawa, S., Gupta, H., 2009. Biological activities of quinoline derivatives. Mini Rev. Med. Chem. 9, 1648–1654.
La Porta, F.A., Ramalho, T.C., Santiago, R.T., Rocha, M.V., da Cunha, E.F., 2011. Orbital signatures as a descriptor of regioselectivity and chemical reactivity: the role of the frontier orbitals on 1, 3-Dipolar cycloadditions. J. Phys. Chem. A 115, 824–833.
Lagunin, A., Stepanchikova, A., Filimonov, D., Poroikov, V., 2000. PASS: prediction of activity spectra for biologically active substances. Bioinformatics 16, 747–748.
Le Bahers, T., Adamo, C., Ciofini, I., 2011. A qualitative index of spatial extent in charge-transfer excitations. J. Chem. Theory Comput. 7, 2498–2506.
Lee, M., Zimmermann-Steffens, S.G., Arey, J.S., Fenner, K., von Gunten, U., 2015. Development of prediction models for the reactivity of organic compounds with ozone in aqueous solution by quantum chemical calculations: the role of delocalized and localized molecular orbitals. Environ. Sci. Technol. 49, 9925–9935.
Lienard, P., Gavartin, J., Boccardi, G., Meunier, M., 2015. Predicting drug substances Autoxidation. Pharm. Res. 32, 300–310.
Lipinski, C.A., 2004. Lead-and drug-like compounds: the rule-of-five revolution. Drug Discov. Today: Technol. 1, 337–341.
Lipinski, C.A., Lombardo, F., Dominy, B.W., Feeney, P.J., 1997. Experimental and computational approaches to estimate solubility and permeability in drug discovery and development settings. Adv. Drug Deliver. Rev. 23, 3–25.
Lu, T., Chen, F., 2012a. Multiwfn: a multifunctional wavefunction analyzer. J. Comput. Chem. 33, 580–592.
Lu, T., Chen, F., 2012b. Quantitative analysis of molecular surface based on improved Marching Tetrahedra algorithm. J. Mol. Graph. Model. 38, 314–323.
Luque, F.J., Lopez, J.M., Orozco, M., 2000. Perspective on electrostatic interactions of a solute with a continuum, a direct utilization of ab initio molecular potentials for the prevision of solvent effects. Theor. Chem. Acc. 103, 343–345.
Makioka, Y., Shindo, T., Taniguchi, Y., Takaki, K., Fujiwara, Y., 1995. Ytterbium(III) triflate catalyzed synthesis of quinoline derivatives from N-arylaldimines and vinyl ethers. Synthesis, 801–804.
Mameli, M., Aragoni, M.C., Arca, M., Caltagirone, C., Demartin, F., Farruggia, G., De Filippo, G., Devillanova, F.A., Garau, A., Isaia, F., 2010. A selective, nontoxic, OFF–ON fluorescent molecular sensor based on 8-hydroxyquinoline for probing Cd2 + in living cells. Chem.-A Eur. J. 16, 919–930.
Mancini, D.T., Souza, E.F., Caetano, M.S., Ramalho, T.C., 2014. 99Tc NMR as a promising technique for structural investigation of biomolecules: theoretical studies on the solvent and thermal effects of phenylbenzothiazole complex. Magn. Reson. Chem. 52, 129–137.
Marella, A., Tanwar, O.P., Saha, R., Ali, M.R., Srivastava, S., Akhter, M., Shaquiquzzaman, M., Alam, M.M., 2013. Quinoline: a versatile heterocyclic. Saudi Pharm. J. 21, 1–12.
Martin, J.M.L., Van Alsenoy, C., 2007. GAR2PED, a Program to Obtain a Potential Energy Distribution from a Gaussian Archive Record. University of Antwerp, Belgium.
Mary, Y.S., Panicker, C.Y., Anto, P.L., Sapnakumari, M., Narayana, B., Sarojini, B.K., 2015. Molecular structure, FT-IR, NBO, HOMO and LUMO, MEP and first order hyperpolarizability of (2E)-1-(2,4-dichlorophenyl)-3-(3,4,5-trimethoxyphenyl)prop-2-en-1-one by HF and density functional methods. Spectrochim. Acta 135, 81–92.
McCall, J.M., TenBrink, R., Kamdar, B.V., Skaletzky, L.L., Perricone, S.C., Piper, R.C., Delehanty, P.J., 1986. 7-(Trifluoromethyl)-4-aminoquinoline hypotensives: novel peripheral sympatholytics. J. Med. Chem. 29, 133–137.
Xiao, Meng, Lu, T., 2015. Generalized Charge Decomposition Analysis (GCDA) Method. J. Adv. Phys. Chem. 4, 111–124.
Menon, V.V., Fazal, E., Mary, Y.S., Panicker, C.Y., Armaković, S., Armaković, S.J., Nagarajan, S., Van Alsenoy, C., 2017. FT-IR, FT-Raman and NMR characterization of 2-isopropyl-5-methylcyclohexyl quinoline-2-carboxylate and investigation of its reactive and optoelectronic properties by molecular dynamics simulations and DFT calculations. J. Mol. Struct. 1127, 124–137.
Merritt, L.L., Duffin, B., 1970. The crystal structures of two derivatives of 8-hydroxyquinoline-5-sulfonic acid, 2-methyl-8-hydroxyquinoline-5-sulfonic acid monohydrate and 7-iodo-8-hydroxyquinoline-5-sulfonic acid. Acta Cryst. B26, 734–744.
Mi, Y.-S., Liang, D.-M., Chen, Y.-T., Luo, X.-B., Xiang, J.-N., 2014. A rhodamine–quinoline type molecular switch as a highly selective sequential sensor for Al 3+ and F− in aqueous solution. RSC Adv. 4, 42337–42345.
Michalak, A., De Proft, F., Geerlings, P., Nalewajski, R., 1999. Fukui functions from the relaxed Kohn-Sham orbitals. J. Phys. Chem. A 103, 762–771.
Molnar, J.J., Agbaba, J., Dalmacija, B., Klašnja, M., Watson, M., Kragulj, M., 2011. Effects of ozonation and catalytic ozonation on the removal of natural organic matter from groundwater. J. Environ. Eng. 138, 804–808.

Molnar, J.J., Agbaba, J.R., Dalmacija, B.D., Klašnja, M.T., Dalmacija, M.B., Kragulj, M.M., 2012. A comparative study of the effects of ozonation and TiO_2-catalyzed ozonation on the selected chlorine disinfection by-product precursor content and structure. Sci. Total Environ. 425, 169–175.

Mphahlele, M.J., Adeloye, A.O., 2013. 4,6,8-Triarylquinoline-3-carbaldehyde derivatives: synthesis and photophysical properties. Molecules 18, 15769–15787.

Mulon, J.B., Destandau, E., Alain, V., Bardez, E., 2005. How can aluminium(III) generate fluorescence? J. Inorg. Biochem. 99 (90), 1749–1755.

Murray, J.S., Sen, K., 1996. Molecular Electrostatic Potential, Concepts and Applications. Elsevier, Amsterdam.

Murray, J.S., Seminario, J.M., Politzer, P., Sjoberg, P., 1990. Average local ionization energiescomputed on the surfaces of some strained molecules. Int. J. Quantum Chem. 38, 645–653.

Muthiah, P.T., Murugesan, S., 2006. Synthesis and crystal structures of lithium 8-hydroxyquinoline-5-sulfonate tetrahydrate. J. Coord. Chem. 59, 1167–1172.

Otero-de-la-Roza, A., Johnson, E.R., Contreras-García, J., 2012. Revealing non-covalent interactions in solids: NCI plots revisited. Phys. Chem. Chem. Phys. 14, 12165–12172.

Panicker, C.Y., Varghese, H.T., Philip, D., Nogueira, H.I.S., Castkova, K., 2007. Raman, IR and SERS spectra of methyl(2-methyl-4,6-dinitrophenylsulfanyl)ethanoate. Spectrochim. Acta 67, 1313–1320.

Park, H.M., Oh, B.N., Kim, J.H., Qiong, W., Hwang, I.H., Jung, K.-D., Kim, C., Kim, J., 2011. Fluorescent chemosensor based-on naphthol–quinoline for selective detection of aluminum ions. Tetrahedron Lett. 52, 5581–5584.

Parr, R.G., Pearson, R.G., 1983. Absolute hardness: companion parameter to absolute electronegativity. J. Am. Chem. Soc. 105, 7512–7516.

Parveen, S., Al-Alshaikh, M.A., Panicker, C.Y., El-Emam, A.A., Narayana, B., Saliyan, V.V., Sarojini, B., Van Alsenoy, C., 2016. J. Mol. Struct. 1112, 136–146.

Perez-Bolivar, C., Montes, V.A., Anzenbachier, P., 2006. True blue: blue emitting Al^{3+} quinolinolate complexes. Inorg. Chem. 45, 9610–9612.

Phillips, M.A., White, K.L., Kokkonda, S., Deng, X., White, J., El Mazouni, F., Marsh, K., Tomchick, D.R., Manjalanagara, K., Rudra, K.R., Wirjanata, G., Noviyanti, R., Price, R.N., Marfurt, J., Shackleford, D.M., Chiu, F.C., Campbell, M., Jimenez-Diaz, M.B., Bazaga, S.F., Angulo-Barturen, I., Martinez, M.S., Lafuente-Monasterio, M., Kaminsky, W., Silue, K., Zeeman, A. M., Kocken, C., Leroy, D., Blasco, B., Rossignol, E., Rueckle, T., Matthews, D., Burrows, J.N., Waterson, D., Palmer, M.J., Rathod, P.K., Charman, S.A., 2016. A triazolopyrimidine-based dihydroorotate dehydrogenase inhibitor with improved drug-like properties for treatment and prevention of Malaria. ACS Infect Dis. http://dx.doi.org/10.1021/acsinfecdis.6b00144.

Phillips, M.A., White, K.L., Kokkonda, S., Deng, X., White, J., El Mazouni, F., Marsh, K., Tomchick, D.R., Manjalanagara, K., Rudra, K.R., 2016. A triazolopyrimidine-based dihydroorotate dehydrogenase inhibitor with improved drug-like properties for treatment and prevention of malaria. ACS Infect. Dis. 2, 945–957.

Politzer, P., Murray, J.S., 1991. In: Beveridge, D.L., Lavery, R., (Eds.), Theoretical Biochemistry and Molecular Biophysics. Springer, Berlin, p. 68.

Politzer, P., Abu-Awwad, F., Murray, J.S., 1998. Comparison of density functional and Hartree-Fock average local ionization energies on molecular surfaces. Int. J. Quantum Chem. 69, 607–613.

Politzer, P., Murray, J.S., Bulat, F.A., 2010. Average local ionization energy: a review. J. Mol. Model. 16, 1731–1742.

Ramalho, T.C., da Cunha, E.F., De Alencastro, R.B., 2004. Solvent effects on 13C and 15N shielding tensors of nitroimidazoles in the condensed phase: a sequential molecular dynamics/quantum mechanics study. J. Phys.: Condens. Matter 16, 6159.

Ramalho, T.C., Martins, T.L., Borges, L.E.P., de Pinho, M.H., de Avillez, R.R., da Cunha, E.F., 2009. Influence of Zn–Cd substitution: spectroscopic and theoretical investigation of 8-hydroxyquinoline complexes. Spectrochim. Acta Part A Mol. Biomol. Spectrosc. 72, 726–729.

Reed, A.E., Curtiss, L.A., Weinhold, F., 1988. Intermolecular interactions from a natural bond orbital, donor acceptor viewpoint. Chem. Rev. 88, 899–926.

Schrödinger Release 2016-4: Maestro, Schrödinger, LLC, New York, NY, 2016. 2015.

Ren, X., Sun, Y., Fu, X., Zhu, L., Cui, Z., 2013. DFT comparison of the OH-initiated degradation mechanisms for five chlorophenoxy herbicides. J. Mol. Model. 19, 2249–2263.

Roeges, N.P.G., 1994. A Guide to the Complete Interpretation of Infrared Spectra of Organic Structures. John Wiley and Sons, New York.

Sangani, C.B., Makawana, J.A., Zhang, X., Teraiya, S.C., Lin, I., Zhu, H.L., 2014. Design, synthesis and molecular modeling of pyrazole-quinoline-pyridine hybrids as a new class of antimicrobial and anticancer agents. Eur. J. Med. Chem. 76, 549–557.

Sang-aroon, W., Amornkitbamrung, V., Ruangpornvisuti, V., 2013. A density functional theory study on peptide bond cleavage at aspartic residues: direct vs cyclic intermediate hydrolysis. J. Mol. Model. 19, 5501–5513.

Sangu, K., Fuchibe, K., Akiyama, T., 2004. A novel approach to 2-arylated quinolines: electrocyclization of alkynyl imines via vinylidene complexes. Org. Lett. 6, 353–355.

Sanner, M.F., Olson, A.J., Spehner, J.-C., 1995. Fast and robust computation of molecular surfaces. In: Proceedings of the eleventh annual symposium on Computational geometry. ACM.

Schleyer, P.v.R., Maerker, C., Dransfeld, A., Jiao, H., Hommes, N.J.v.E., 1996. Nucleus-independent chemical shifts: a simple and efficient aromaticity probe. J. Am. Chem. Soc., 118, 6317–6318.

Schrödinger Release 2017-2: MacroModel, Schrödinger, LLC, New York, NY, 2017..

Seminario, J.M., 1996. In: Recent Development and Applications of Modern Density Functional Theory, vol. 4. Elsevier.

Senthilkumar, P., Dinakaran, M., Yogeeswari, P., Sriram, D., China, A., Nagaraja, V., 2009. Synthesis and antimycobacterial activities of novel 6-nitroquinolone-3-carboxylic acids. Eur. J. Med. Chem. 44, 345–358.

Sharma, R., Zeller, M., Pavlovic, V.I., Huang, T.S., Lo, Z., Chu, S., Zhao, Y., Phillips, J.C., Schulten, K., 2000. Speech/gesture interface to a visual-computing environment. IEEE Comput. Graphics Appl. 20, 29–37.

Shen, Y.R., 1984. The Principles of Nonlinear Optics. Wiley, New York.

Shivakumar, D., Williams, J., Wu, Y., Damm, W., Shelley, J., Sherman, W., 2010. Prediction of absolute solvation free energies using molecular dynamics free energy perturbation and the OPLS force field. J. Chem. Theor. Comput. 6, 1509–1519.

Silverstein, R.M., Bassler, G.C., Morril, T.C., 1991. Spectrometric Identification of Organic Compounds. John Wiley and Sons Inc., Singapore.

Sircar, I., Haleen, S.J., Burke, S.E., Barth, H., 1992. Synthesis and biological activity of 4-(diphenylmethyl)-. alpha.-[(4-quinolinyloxy) methyl]-1-piperazineethanol and related compounds. J. Med. Chem. 35, 4442–4449.

Smith, G., Wermuth, U.D., Healy, P.C., 2007. Proton transfer compounds of 8-hydroxy-7-iodoquinoline-5-sulfonic acid (ferron) with 4-chloroaniline and 4-bromoaniline. Acta Cryst. C63, o405–407.

Socrates, G., 2001. Infrared and Raman Characteristic Group Frequencies. Wiley, Middlesex, UK.

Sroka, Z., Żbikowska, B., Hładyszowski, J., 2015. The antiradical activity of some selected flavones and flavonols. Experimental and quantum mechanical study. J. Mol. Model. 21, 1–11.

Stone, J.E., Gullingsrud, J., Schulten, K., 2001. A system for interactive molecular dynamics simulation. In: Proceedings of the 2001 symposium on Interactive 3D graphics. ACM.

Swenson, R.E., Sowin, T.J., Zhang, H.Q., 2002. Synthesis of substituted quinolines using the dianion addition of N-Boc-anilines and α-tolylsulfonyl-α, β-unsaturated ketones. J. Org. Chem. 67, 9182–9185.

Tachikawa, H., Igarashi, M., Ishibashi, T., 2002. Ab initio molecular dynamics (MD) calculations of hyperfine coupling constants of methyl radical. Chem. Phys. Lett. 352, 113–119.

Taha, M., Ismail, N.H., Imran, S., Wadood, A., Rahim, F., Ali, M., Rehman, A.U., 2015. Novel quinoline derivatives as potent in vitro α-glucosidase inhibitors: in silico studies and SAR predictions. MedChemComm 6, 1826–1836.

Taha, M., Sultan, S., Nuzar, H.A., Rahim, F., Imran, S., Ismail, N. H., Naz, H., Ullah, H., 2016. Synthesis and biological evaluation of novel N-arylidenequinoline-3-carbohydrazides as potent β-glucuronidase inhibitors. Biorg. Med. Chem. 24, 3696–3704.

Tian, L.¸Feiwu, C., 2011. Calculation of molecular orbital composition.

Tian, Y.P., Yu, W.T., Zhao, C.Y., Jiang, M.H., Cari, Z.G., Fun, H. K., 2002. Structural characterization and second order nonlinear optical properties of zinc halide thiosemicarbazone complexes. Polyhedron 21, 1217–1222.

Trott, O., Olson, A.J., 2010. AutoDock Vina: improving the speed and accuracy of docking with a new scoring function, efficient optimization and multithreading. J. Comput. Chem. 31, 455–461.

Ulahannan, R.T., Panicker, C.Y., Varghese, H.T., Musiol, R., Josef, J., Van Alsenoy, C., War, J.A., Al-Saadi, A.A., 2015. Vibrational spectroscopic and molecular docking study of (2E)-N-(4-chloro-2-oxo-1,2-dihydroquinoline-3-yl]-3-phenylprop-2-enamide. Spectrochim. Acta 151, 335–349.

Ulahannan, R.T., Panicker, C.Y., Varghese, H.T., Musiol, R., Josef, J., Van Alsenoy, C., War, J.A., Srivastava, S.K., 2015. Molecular structure, FT-IR, FT-Raman, NBO, HOMO and LUMO, MEP, NLO and molecular docking study of 2-[(E)-2-(2-bromophenyl)-ethenyl]quinoline-6-carboxylic acid. Spectrochim. Acta 151, 184–197.

van der Wijst, T., Fonseca Guerra, C., Swart, M., Bickelhaupt, F.M., Lippert, B., 2009. Rare tautomers of 1-methyluracil and 1-methylthymine: tuning relative stabilities through coordination to PtII complexes. Chem.-A Eur. J. 15, 209–218.

Varsanyi, G., 1974. Assignments for Vibrational Spectra of Seven Hundred Benzene Derivatives. Wiley, New York.

Varshney, Amitabh, Frederick, J., Brooks, P., Wright, W.V., 1994. Linearly Scalable Computation of Smooth Molecular Surfaces. In: IEEE Computer Graphics and Applications.

Veber, D.F., Johnson, S.R., Cheng, H.-Y., Smith, B.R., Ward, K.W., Kopple, K.D., 2002. Molecular properties that influence the oral bioavailability of drug candidates. J. Med. Chem. 45, 2615–2623.

Viswanadhan, V.N., Ghose, A.K., Revankar, G.R., Robins, R.K., 1989. Atomic physicochemical parameters for three dimensional structure directed quantitative structure-activity relationships. IV: additional parameters for hydrophobic and dispersive interactions and their application for an automated superposition of certain naturally occurring nucleoside antibiotics. J. Chem. Inform. Comput. Sci., 29, 163–172.

Wang, H., Wang, W.S., Zhang, H.S., 2001a. A spectrofluorimetric method for cysteine and glutathione using the fluorescence system of Zn(II)-8-hydroxyquinoline-5-sulphonic acid complex. Spectrochim. Acta A 57 (12), 2403–2407.

Wang, Y., Astilean, S., Haran, G., Warshawsky, A., 2001b. Microenvironmental investigation of polymer bound fluorescent chelator by fluorescence microscopy and optical spectroscopy. Anal. Chem. 73 (17), 4096–4103.

Weinhold, F., Landis, C.R., 2001. Chem. Ed: Res & Pract 2 (CERP; special "structural concepts" issue), 91–104.

Wright, C.W., Addae-Kyereme, J., Breen, A.G., Brown, J.E., Cox, M.F., Croft, S.L., Gökçek, Y., Kendrick, H., Phillips, R.M., Pollet, P.L., 2001. Synthesis and evaluation of cryptolepine analogues for their potential as new antimalarial agents. J. Med. Chem. 44, 3187–3194.

Wright, J.S., Shadnia, H., Chepelev, L.L., 2009. Stability of carbon–centered radicals: effect of functional groups on the energetics of addition of molecular oxygen. J. Comput. Chem. 30, 1016–1026.

Yanai, T., Tew, D.P., Handy, N.C., 2004. A new hybrid exchange–correlation functional using the Coulomb-attenuating method (CAM-B3LYP). Chem. Phys. Lett. 393, 51–57.